UNIVERSITÉ DU QUÉBEC À MONTRÉAL

LES COMPOSANTES REPRODUCTIBLES ET NON-REPRODUCTIBLES DANS UN ENSEMBLE DE SIMULATIONS PAR UN MODÈLE RÉGIONAL DU CLIMAT

MÉMOIRE

PRÉSENTÉ COMME EXIGENCE PARTIELLE

DE LA MAÎTRISE EN SCIENCES DE L'ATMOSPHÈRE

PAR

LEO SEPAROVIC

NOVEMBRE 2007

UNIVERSITÉ DU QUÉBEC À MONTRÉAL

REPRODUCIBLE AND IRREPRODUCIBLE COMPONENTS IN ENSEMBLE SIMULATIONS WITH A REGIONAL CLIMATE MODEL

THESIS

PRESENTED IN PARTIAL FULLFILMENT

OF THE REQUIREMENTS FOR THE MASTER'S DEGREE

IN ATMOPSHERIC SCIENCES

BY

LEO SEPAROVIC

NOVEMBER 2007

REMERCIEMENTS

Premièrement, je remercie mon directeur de recherche, M. René Laprise, pour l'opportunité de participer à ce projet. Je le remercie profondément pour tous les conseils et discussions qui ont guidé mon activité scientifique et sans lesquels le présent mémoire n'aurait pas pu exister.

Je remercie mon codirecteur M. Ramón de Elía, pour son important appui scientifique, pour sa patience et, particulièrement, pour les longues discussions qui ont approfondi mes connaissances sur la variabilité interne des modèles régionaux de climat.

Je tiens aussi à remercier beaucoup Mlle Adelina Alexandru car elle a généré et analysé systématiquement une immense base de donnée qui se trouve à la base de cette recherche. Finalement, je remercie M. Martin Leduc pour les discussions scientifiques reliées à ce sujet et, particulièrement, pour son appui d'apprendre rapidement les outils et logiciels informatiques nécessaires.

TABLE DES MATIÈRES

LISTE DES FIGURES

Figure ***Page***

LISTE DES ABRÉVIATIONS

AMIP	*Atmospheric Model Intercomparison Project*
CFL	Conditions aux Frontières Latérales
CI	Conditions Initiales
CRCM	*Canadian Regional Climate Model*
DCT	*Discrete Cosine Transform*
ECMWF	*European Center for Medium-range Weather Forecasts*
GCM	*Global Circulation Model*
IC	*Initial Conditions*
LAM	*Limited Area Model*
LBC	*Lateral Boundary Conditions*
MCG	Modèle de Circulation Générale
MRC	Modèle Régional du Climat
MRCC	Modèle Régional Canadien du Climat
MSD	*Mean Square Difference*
NCEP	*National Center for Environmental Prediction*
RCM	*Regional Climate Model*
SST	*Sea Surface Temperature*
UTC	*Coordinated Universal Time*

LISTE DES SYMBOLES

i	Index zonale du point de grille
j	Index méridionale du point de grille
k	Index d'échantillonnage des champs simulés
K	Nombre d'échantillons
l	Longueur d'onde
M	Nombre de simulations dans l'ensemble (20)
N	Nombre de points de grille dans la direction zonale ou méridionale (101)
q	Nombre d'onde
S	Puissance spectrale
S^A	Moyenne d'ensemble des puissances spectrales générées par les membres d'ensemble
S^I	Puissance spectrale de la composante non-reproductible
S^R	Puissance spectrale de la composante reproductible
S^D	Puissance spectrale des analyses NCEP
t	Temps
t_0	Temps du début de la saison étudiée (1ère Juillet 1993)
Δt	Intervalle d'échantillonnage (6 heures)
$\langle X \rangle$	Moyenne d'ensemble d'une variable X
X^*	Déviation d'une variable X par rapport à la moyenne d'ensemble
ε	Écart type par rapport à la moyenne d'ensemble
η	Variance accrue
Δ	Espacement de grille
ρ	Rapport de reproductibilité
σ^2	Variance des perturbations transitoires
σ^{2A}	Moyenne d'ensemble des variances des perturbations transitoires des membres de l'ensemble

σ^{2I} Variance des perturbations transitoires de la composante reproductible

σ^{2R} Variance des perturbations transitoires de la composante non-reproductible

RÉSUMÉ

L'objectif de la mise à l'échelle dynamique par les Modèles Régionaux du Climat (MRC) est de générer une variabilité spatio-temporelle de fine échelle à partir des champs à faible résolution. La plupart des MRC sont définis comme un problème de conditions aux frontières, où les Conditions aux Frontières Latérales (CFL) sont définies à partir des champs de pilotage à faible résolution.

La variabilité interne des modèles régionaux met en question l'unicité de sa solution. Une petite différence, aux petites échelles des spectres des champs simulés, se propage vers les échelles plus grandes, et ajoute une composante aléatoire au signal forcé. Au même moment, l'advection de l'information prescrite par les conditions aux frontières latérales vers l'intérieur du domaine contraint la partie forcée de la solution du modèle.

Par conséquent la variabilité spatio-temporelle générée par les MRC se compose d'une composante reproductible associée au forçage externe, *i.e.* le forçage exercé par l'extérieur sur l'atmosphère simulée, et d'une composante non-reproductible, associée à la variabilité interne. La présente étude examine comment un MRC partage sa variabilité spatio-temporelle entre les deux composantes.

L'analyse est basée sur un ensemble de 20 simulations, effectuée par le Modèle Régional Canadien du Climat (MRCC) pour une saison d'été. Les simulations sont pilotées par les réanalyses NCEP. La composante reproductible est identifiée par la moyenne d'ensemble tandis que la composante non-reproductible est échantillonnée à partir des déviations des membres de l'ensemble par rapport à la moyenne d'ensemble.

Quand les champs instantanés sont étudiés, les résultats montrent que la variabilité interne dépend fortement de l'échelle spatiale; les plus petites échelles sont les plus affectées. Aux grandes échelles de l'ordre de *1000km*, la composante reproductible est beaucoup plus grande que la composante non-reproductible. Par contre, aux échelles de l'ordre de *100km*, la composante non-reproductible n'est plus négligeable.

Les profils verticaux de la reproductibilité indiquent que, dans l'ensemble étudié, le forçage par la surface ne contraint pas la circulation du modèle considérablement. La distribution géographique montre, pour les grandes échelles de toutes les variables, le même patron spatial de la reproductibilité: La reproductibilité est en général grande à proximité des frontières d'entrée et elle diminue en aval. La distribution spatiale de reproductibilité des petites échelles suit principalement celle des grandes échelles, mais les valeurs sont considérablement plus petites. De même, la variation temporelle de la reproductibilité des petites échelles est relativement bien synchronisée avec celle de la reproductibilité de grandes échelles. Cela implique que les reproductibilités des grandes et petites échelles sont liées.

L'analyse des moyennes saisonnières montre que la composante reproductible domine le spectre entier. Cependant, aux échelles plus petites que 200km, la composante non-reproductible devient non négligeable.

Additionnement, la variabilité spatiale du MRCC aux grandes échelles est en moyenne légèrement surestimée par rapport aux analyses objectives près de la surface. Par contre, elle est sous-estimée dans la troposphère supérieure. Ceci justifie le besoin d'appliquer le pilotage des grandes échelles à l'intérieur du domaine du MRCC.

Mots-clés : Modèles Régionaux du Climat, variabilité interne, « dynamical downscaling ».

ABSTRACT

The fact that Regional Climate Model (RCM) variables can be affected by internal chaotic variations implies that a part of the downscaled information is irreproducible and should be treated in stochastic manner. On the other hand, being constrained by externally provided large-scale information prescribed at the lateral boundaries and forced by high-resolution surface conditions, RCMs might provide a part of their fine-scale downscaled information as independent of perturbations in the initial conditions and in this sense reproducible.

A twenty-member ensemble of the Canadian Regional Climate Model (CRCM) simulations with perturbed initial conditions is conducted for one summer season over a large mid-latitude domain with lateral boundary conditions derived from NCEP reanalyses. The time-dependent ensemble mean is regarded as the reproducible component associated with lateral boundary and surface forcing. The departures from the ensemble mean are used to sample the irreproducible component of the spatiotemporal variability. Relative contributions of these two components to the simulated spatiotemporal variability are examined by means of their geographical distribution, time variation and spectral behaviour.

When instantaneous atmospheric states are considered, results show that large scales are dominated by variability of reproducible nature. At scales between 1000 and 200 km reproducibility depends strongly on the model variable and weather pattern. The fine-scale features are dominated by the irreproducible component. Only a slight increase of reproducibility is noticed at low levels. Oceanic and continental regions are associated with distinct vertical profiles of the relative magnitude of the irreproducible component, which suggests the link between convection over the warm continental surface and internal model variability. Spatial and temporal variations of reproducibility of large and small scales correlate, which implies that reproducibility of small scales could be conditioned by reproducibility of the large-scale flow. For seasonal averages results show little spatial variability in the irreproducible form, with exception of precipitation that retains non-negligible values of its irreproducible component at small scales.

Key words: Regional Climate Models, internal variability, dynamical downscaling.

INTRODUCTION

Les Modèles de Circulation Générale (MCG) de l'atmosphère sont des outils nécessaires pour étudier la variabilité naturelle de l'atmosphère et sa sensibilité aux forçages externes. Les simulations du système climatique par les MCG incluent le couplage de l'atmosphère avec le sol, l'océan et la glace de mer. Afin de bien représenter les processus physiques et le forçage par la frontière inférieure et supérieure, il est nécessaire d'effectuer des simulations à haute résolution. Néanmoins, la complexité des MCG, la grandeur du domaine global et le besoin d'ensemble de simulations pour réaliser des estimations statistiquement robustes imposent un coût informatique énorme pour effectuer des simulations globales à haute résolution (de l'ordre de 10 km). Par contre, les Modèles Régionaux du Climat (MRC) introduits par Giorgi et Bates (1989) permettent de réaliser des simulations à plus haute résolution à un coût informatique accessible.

Les MRC constituent une version des modèles atmosphériques où l'effort informatique est concentré à simuler le climat à haute résolution pour une région spécifiée du globe ; voir Giorgi et Mearns (1999). La plupart de MRC sont définis comme des Modèles à Aire Limitée (*Limited Area Model* - LAM) dont les simulations présentent la solution d'un problème aux frontières (*boundary-value problem*). Dans ce cas, les Conditions aux Frontières Latérales (CFL) sont dérivées à partir des champs de pilotage à faible résolution provenant soit d'analyses objectives (pour la validation des simulations du climat passé) ou de simulations de MCG ou MRC (climat passé ou futur).

L'approche la plus populaire du traitement des CFL est la relaxation des variables du MRC vers les champs de pilotage dans une zone le long de ses frontières latérales, sans rétroactions du modèle vers les champs pilotés (Davies, 1976). Cette approche est aussi appelée mise à l'échelle dynamique parce que les MRC sont supposés être capables de

générer de la variabilité de petite échelle qui n'est pas résolue par les champs de pilotage (Laprise *et al.*, 2000 et de Elía *et al.*, 2002).

Néanmoins, lorsque le pilotage est uniquement effectué par les frontières latérales et non à l'intérieur du domaine, plusieurs études montrent que l'écoulement de grande échelle des MRC peut dévier de celui qui est prescrit par ces CFL (*e.g.* Alexandru *et al.*, 2007). Von Storch *et al.* (2000) ont suggéré un pilotage spectral des grandes échelles. Par exemple, Miguez-Macho *et al.* (2004) ont rapporté que la précipitation était mieux simulée quant ils appliquaient le pilotage spectral dans leurs simulations.

L'objectif d'effectuer la mise à l'échelle dynamique par les MRC est d'ajouter une variabilité spatio-temporelle de fine échelle aux champs de faible résolution du pilote. Toutefois, il est bien connu que les modèles atmosphériques montrent un comportement chaotique. Les deux trajectoires dans l'espace de phase, qui décrivent deux histoires initialement presque identiques d'un système chaotique, divergent avec le temps. La nature chaotique du système met en question l'unicité de la solution d'une simulation régionale.

Dans les ensembles de simulations des MCG, générées par des petites perturbations dans les Conditions Initiales (CI), la variance des membres de l'ensemble par rapport à leur moyenne augmente généralement avec le temps jusqu'à ce qu'elle devienne saturée à une valeur approximativement égale à la variance temporelle des perturbations transitoires. Ce phénomène s'appelle la variabilité interne du système climatique et elle peut être associée aux interactions non-linéaires entre les échelles différentes de mouvement atmosphérique et aux instabilités hydrodynamiques. Une petite différence, aux petites longueurs d'onde des spectres des champs des MCG, se propage vers les longueurs d'onde plus grandes et éventuellement affecte toutes les échelles du mouvement atmosphérique. Cela rend les champs instantanés des MCG imprévisibles au-delà de quelques semaines ou mois (*e.g.* Lorenz, 1969 ; Lorenz, 1982 ; Boer, 1984 ; Schubert et Suarez, 1989).

Dans les LAM, le forçage aux frontières provient non seulement de la frontière inférieure, mais aussi des frontières latérales. Plusieurs études de la prévisibilité dans les LAM montrent que les différences entre deux simulations pilotées par les mêmes CFL et à

partir des CI légèrement perturbées tendent à des valeurs beaucoup plus petites que celles qui caractérisent les MCG. Ces valeurs dépendent de la taille du domaine. Ceci a mené Anthes *et al.* (1985) à conclure que les LAM sont caractérisés par une « prévisibilité étendue ». Dans plusieurs études, ce phénomène est attribué à l'advection de l'information des grandes échelles prescrites aux frontières vers l'intérieur du domaine (*e.g.* Vukicevic et Paegle, 1989; Vukicevic et Errico, 1990). Le forçage par la frontière inférieure pourrait aussi contribuer à la « prévisibilité étendue » (van Tuyl et Errico, 1989).

Cependant, l'analyse d'échelle de la croissance de l'erreur de prévision déterministe dans les LAM montre que l'erreur contamine rapidement la région spectrale des petites échelles (Laprise *et al.*, 2000 ; de Elía *et al.*, 2002). Ceci implique que la « prévisibilité étendue » puisse être la propriété exclusive des grandes échelles. Il faut aussi noter que la conclusion mentionnée ci-dessus ne s'applique pas nécessairement aux statistiques saisonnières des variables des MRC. Denis *et al.* (2002) ont montré qu'une simulation de MRC à haute résolution pilotée par une autre simulation provenant du même modèle sur un domaine plus grand, dont les petites échelles étaient filtrées, avait bien recréé les statistiques mensuelles ou de plus longes échelle temporelle de la simulation utilisée pour le pilotage (comme la moyenne mensuelle et la variance temporelle).

La variabilité interne dans les MRC a commencé à être étudiée récemment. Giorgi et Bi (2000) ont effectué des simulations identiques de MRC, pour chacune des quatre saisons de l'année. L'ensemble a été généré en imposant des perturbations des différentes amplitudes aux CI ou aux CFL. La variabilité interne d'une simulation perturbée a été évaluée comme la moyenne spatiale de la différence quadratique entre cette dernière et la simulation de base correspondante qui n'était pas perturbée. Les résultats de cette étude montrent que la variabilité interne ne dépend ni de la source ni de la magnitude des perturbations, car dans tous les cas elle avait la même évolution temporelle et la même intensité.

Plusieurs études récentes de la variabilité interne montrent que la dispersion instantanée des membres d'ensembles peut varier considérablement selon la saison. Giorgi *et* Bi (2000) et Caya *et* Biner (2004) ont trouvé qu'elle était maximale pendant l'été et minimale pendant l'hiver pour un domaine aux latitudes moyennes. La variabilité interne dans leurs

simulations a été moins intense que celle d'un MCG, sauf pendant l'été, quand elle a été par intermittence comparable à la variabilité interne des MCG. La variabilité interne dans un domaine arctique peut être beaucoup plus intense que dans les simulations conduites sur des domaines aux latitudes moyennes de taille comparable et son cycle saisonnier peut exprimer un maximum en automne et hiver (Rinke *et al.*, 2004).

La grandeur du domaine des MRC influence aussi leur variabilité interne. Alexandru *et al.* (2007) ont étudié les ensembles de simulations d'un MRC, effectuées pour plusieurs domaines des différentes tailles, couvrant la côte est de l'Amérique du Nord. Les changements de la taille du domaine ont changé considérablement la distribution spatiale et la magnitude de la variabilité interne. Une augmentation de la taille du domaine a augmenté généralement la variabilité interne. Cette étude a montré aussi la dépendance de sa distribution géographique de variable simulée. Le maximum de la variabilité interne de la précipitation a été associé aux régions auxquelles la convection était fréquente. La région de maximum de la variabilité interne de la hauteur géopotentiel a été située plus en aval de ces régions. De plus, la dispersion des réalisations des moyennes saisonnières a été beaucoup plus petite, mais, en cas de précipitation, elle a été localement comparable à celles qui sont vues dans les MCG. Jones *et al.* (1997), Christensen *et al.* (2001), Rinke *et al.* (2004) et de Elía *et al.* (2007) ont aussi noté que les moyennes saisonnières sont affectées par la variabilité interne.

On peut donc résumer les différences de variabilité des MCG et MRC comme suit. Dans les MCG, la variabilité spatio-temporelle est presque entièrement générée par la composante variable et donc elle est presque non-reproductible dans un sens déterministe. Néanmoins, un certain nombre d'équipes de recherche ont généré des ensembles d'intégrations multiples de MCG non-couplés, dont plusieurs étaient dans le cadre d'expérience AMIP (*Atmospheric Model Intercomparison Project*, *e.g.* Gates, 1992). Dans ce contexte, on prescrit le forçage externe par les données des anomalies de la température de surface de la mer et on laisse ce forçage influencer l'évolution des simulations d'ensemble. Par cette approche, Stern *et* Miyakoda (1995) ont montré que, dans certaines régions tropicales, la composante reproductible de la variabilité interannuelle n'était pas négligeable dans leur simulation de MCG. Une variation interannuelle du forçage exercée par la surface

de l'océan rend donc une partie de la variabilité interannuelle du climat prévisible par les MCG.

Le pilotage par des CFL dans les MRC représente un forçage additionnel qui peut contraindre considérablement leur variabilité interne. Par conséquent la variabilité spatiale des champs instantanés des MRC est partagée entre les composantes reproductible et non-reproductible. L'information imposée aux frontières latérales contient seulement les grandes échelles spatio-temporelles car la résolution des champs de pilotage est faible. Par contre, la haute résolution des MRC permet que le forçage par la frontière inférieure contienne des petites échelles. L'hypothèse de ce mémoire est que l'interaction dynamique entre les grandes échelles fournies aux frontières latérales et le forçage de petite échelle effectué par le MRC rend reproductible une partie de la variabilité spatio-temporelle de fine échelle.

Le présent mémoire approfondit l'étude de la variabilité interne dans les MRC. L'intérêt principal est la capacité des MRC de produire un signal unique, indépendant des perturbations dans les CI, et résultant du forçage par les frontières. Les ensembles de simulations permettent une décomposition de la variabilité spatiotemporelle générée par le modèle dans deux composantes : (1) la composante reproductible associée au forçage externe, *i.e.* le forçage exercé par l'extérieur sur l'atmosphère simulée, et (2) la composante non-reproductible, associée à la variabilité interne.

L'analyse est basée sur un ensemble de 20 simulations, effectuée par Alexandru *et al.* (2007), sur un domaine centré aux latitudes moyennes pour la saison d'été de l'année 1993. Les simulations sont pilotées par les analyses NCEP (*National Centers for Environmental Prediction*). Le modèle est piloté dans une bande de 9 points le long des frontières latérales. Aucun pilotage n'a été effectué à l'intérieur du domaine.

L'analyse des résultats est présentée sous forme d'un article rédigé en anglais. Dans la première partie de l'article, on décrit l'ensemble de simulations et on définit les composantes reproductibles et non-reproductibles. Par la suite, le comportement spectral de la reproductibilité est analysé. Cela définit la façon dont la variabilité spatiale est divisée entre les deux composantes par rapport à l'échelle spatiale. Ensuite, la distribution géographique de

la reproductibilité est étudiée. La dernière partie de l'étude décrit l'analyse de l'effet de la variabilité interne sur les moyennes saisonnières.

CHAPITRE I

LES COMPOSANTES REPRODUCTIBLES ET NON-REPRODUCTIBLES DANS UN ENSEMBLE DE SIMULATIONS PAR UN MODÈLE RÉGIONAL DU CLIMAT

Ce chapitre, présenté sous forme d'un article rédigé en anglais, est une étude de la variabilité interne du Modèle Régional Canadien du Climat (MRCC). Le chapitre contient aussi des informations sur le MRCC et l'ensemble de simulations et la méthodologie appliquée.

Reproducible and Irreproducible Components in Ensemble Simulations with a Regional Climate Model

by

Leo Separovic [1], Ramon de Elía [2] and René Laprise [1]

Canadian Network for Regional Climate Modelling and Diagnostics

(1) Université du Québec à Montréal
(2) Ouranos Consortium

November 2007

Corresponding author's address:

Leo Separovic
UQAM
Ouranos, 550 Sherbrooke St West, 19th floor, West Tower
Montréal (Québec) Canada H3A 1B9
E-mail: separovi@sca.uqam.ca

Abstract

The fact that Regional Climate Model (RCM) variables can be affected by internal chaotic variations implies that a part of the downscaled information is irreproducible and should be treated in stochastic manner. On the other hand, being constrained by externally provided large-scale information prescribed at the lateral boundaries and forced by high-resolution surface conditions, RCMs might provide a part of their fine-scale downscaled information as independent of perturbations in the initial conditions and in this sense reproducible.

A twenty-member ensemble of the Canadian Regional Climate Model (CRCM) simulations with perturbed initial conditions is conducted for one summer season over a large mid-latitude domain with lateral boundary conditions derived from NCEP reanalyses. The time-dependent ensemble mean is regarded as the reproducible component associated with lateral boundary and surface forcing. The departures from the ensemble mean are used to sample the irreproducible component of the spatiotemporal variability. Relative contributions of these two components to the simulated spatiotemporal variability are examined by means of their geographical distribution, time variation and spectral behaviour.

When instantaneous atmospheric states are considered, results show that large scales are dominated by variability of reproducible nature. At scales between 1000 and 200 km reproducibility depends strongly on the model variable and weather pattern. The fine-scale features are dominated by the irreproducible component. Only a slight increase of reproducibility is noticed at low levels. Oceanic and continental regions are associated with distinct vertical profiles of the relative magnitude of the irreproducible component, which suggests the link between convection over the warm continental surface and internal model variability. Spatial and temporal variations of reproducibility of large and small scales correlate, which implies that reproducibility of small scales could be conditioned by reproducibility of the large-scale flow. For seasonal averages results show little spatial

variability in the irreproducible form, with exception of precipitation that retains non-negligible values of its irreproducible component at small scales.

1. Introduction

Since the beginning of numerical weather prediction (NWP) of the atmosphere, there has been rapidly growing evidence that atmospheric models display chaotic behaviour. Two neighbouring trajectories in phase space diverge in time at a rate that depends on the initial state and characteristics of the system. Experimental evidence shows that, in ensembles of global model integrations generated with slightly perturbed initial conditions, the inter-member variance increases in time until it becomes saturated at a value approximately equal to the climatological temporal variance. From that time onward, realizations of the ensemble are on average uncorrelated. Boer (1984) showed that the small-scale error induced by uncertainties in global model Initial Conditions (IC) and model structural simplifications grow in time and propagate upscale through the spectrum eventually affecting all length scales. It is generally accepted that, due to their internal variability, time-dependent eddies in the large-scale flow are unpredictable by global models beyond few weeks or a month (*e.g.* Lorenz, 1969; Lorenz, 1982; Schubert et Suarez, 1989).

The distinct feature of Limited-Area Models (LAMs) (see Giorgi and Mearns, 1999, for a review), in addition to their high resolution, is their need for information at the boundaries of their domain of integration. The most popular approach of lateral boundary treatment in LAMs has been so far the "one-way" nesting strategy. This method involves the relaxation of the LAM high-resolution variables in the vicinity of the boundary to the externally prescribed coarse-resolution variables, with no feedback permitted from the LAM to the driving fields (e.g. Davies and Turner, 1977).

Studies of predictability of high-resolution nested LAMs show that, for smaller domains, variance among model runs, generated by the identical Lateral Boundary Conditions (LBC) and perturbed IC, asymptotes to values much smaller than those obtained by global models. This phenomenon was referred to as "extended LAM predictability" by Anthes et al. (1985) and has been mainly attributed to advection of information on the large-

scale flow, prescribed at LAM lateral boundaries, towards the interior of the LAM domain (e.g. Vukicevic and Paegle, 1989; Vukicevic and Errico, 1990). Additionally, it has been suggested that surface forcing exerted by topography and surface heterogeneities, such as soil moisture gradients, might contribute to "extended predictability" in LAMs (van Tuyl and Errico, 1989). It is worth noting that an analogous effect of topographical forcing was documented in studies of predictability in autonomous global models. For example, Boer (1984) attributed an enhanced forecast skill limit of the former ECMWF T213L31 analysis-forecast system at the meso-alpha range to the topographical stationary forcing.

The early experimental evidence that internal chaotic variations might be constrained by external (lateral boundary and surface) forcing in LAMs contributed to the "optimistic" belief that LAMs might deliver unique solution even at scales smaller than those resolved by their driving fields. However, Laprise et al. (2000) and De Elía et al. (2002) suggested that, from a deterministic point of view, dynamical downscaling by LAMs is not very efficient, because forecast errors quickly contaminated spectral range of fine scales within the first several hours of simulations. The "extended predictability" was found confined mainly to the large-scale part of the spectrum that drives the LAM.

Study of internal variability in limited-area Regional Climate Models (RCM) began recently. Due to large computational cost of ensembles of high-resolution RCM simulations, internal RCM variability has been mainly studied utilizing small ensembles.

Weisse et al. (2000) showed that internal variability could be a nuisance in studies of sensitivity of RCM simulations to parameter changes. Giorgi and Bi (2000) conducted ensembles of seasonal RCM simulations over a large mid-latitude domain for each three-month season of a year. Perturbations of different magnitude were imposed to either the IC or the LBC of the control integration. The internal model variability was defined as the time-dependent Mean Square Difference (MSD) between perturbed simulations and the control run. The results revealed the fact that RCMs are characterized by an intrinsic level of internal variability, independent of the origin (LBC or IC) and magnitude of perturbations. The internal variability generally increased during a spin-up period of the order of 10 days after the initialization and then reached a state of dynamical equilibrium. The authors also found

that the MSD varied with seasons and weather regimes, exhibiting a maximum in summer and a minimum in winter.

Caya and Biner (2004) reported a similar annual cycle of internal variability in their three-member ensemble of RCM simulations over a large mid-latitude domain. Their simulations were considerably affected by internal variability revealed as a lack of correlation between the members at specific time. On the other hand, the authors found little difference among the members for climate statistics such as seasonal average and temporal variance. However, an important exception was found for precipitation whose seasonal statistics were notably affected by internal variability. Jones et al. (1997) also found that RCM climate statistics were affected by internal variability in their simulations.

Christensen et al. (2001) reported that magnitude of internal variability of seasonal averages of hydrologically relevant variables was comparable to internal variability in global models. The authors also provided evidence that internal variability depends on model characteristics and integration area.

Based on an RCM simulation nested within the larger-domain simulation of the same model, Denis et al. (2002) showed that the smaller-domain integration accurately recreated the small-scale statistics such as the monthly mean and the temporal variance of the larger-domain simulation, especially in regions of strong topographical forcing. Somewhat less success in small-scale reproducibility was noted over the ocean and away from surface.

Rinke et al. (2004) studied an ensemble of annual integrations over a circumpolar Arctic domain and found internal variability to be much more important than in simulations conducted on mid-latitude domains of comparable size. Additionally, the seasonal cycle of internal variability had very distinct annual cycle over the Arctic domain, with maximum in autumn and winter.

Alexandru et al. (2007) performed a systematic study of RCM internal variability with a 20-member ensemble of one summer-season RCM integrations, conducted over several domains of different sizes, covering the East Coast of North America. The authors found that internal variability displays preferential regions within the domain, depending on the

variable. For example, the maximum scatter in six-hourly mean precipitation occurred in the southeast of United States and was associated to convection in the moist air advected from the Gulf of Mexico over the warm continental surface. Spread in seasonal average precipitation was locally comparable to that in Global Circulation Models (GCM). The maximum spread in instantaneous geopotential height was found downstream of the area of the maximum scatter in precipitation. The authors suggested that the intense convection triggered small-scale perturbations in the mass field that grew in magnitude and increased in length-scale while being advected by the general circulation. Changes in domain size altered considerably the geographical distribution and magnitude of internal variability both for time-dependent model variables and their seasonal averages.

The aforementioned findings about internal variability in nested models have important consequences on the concept of dynamical downscaling. The fact that RCM variables can be affected by internal chaotic variations implies that a part of the downscaled information should be considered in stochastic form. On the other hand, being constrained by large-scale information prescribed at the lateral boundaries and forced by high-resolution surface conditions, RCMs might provide a part of their fine-scale variability in form of an externally forced signal, independent of perturbations in the IC and in this sense reproducible.

Such a concept has been adopted, for example, in studies of predictability with atmospheric GCMs. Several groups associated with the Atmospheric Model Intercomparison Project (AMIP) (e.g. Gates, 1992) conducted ensembles of multiyear GCM simulations with prescribed sea surface temperature (SST) and sea ice. A reproducible seasonal-scale climate signal was then assessed by departures of the ensemble-mean seasonal-average from the GCM multiyear average for that season. The externally forced, reproducible signal was then compared with internal variability measured by the variance of the ensemble of GCM seasonal averages. It has been shown within such an approach that prescribed SST anomalies can induce, especially at low latitudes, a statistically significant reproducible signal in GCM seasonal averages (e.g. Stern and Miyakoda, 1995).

The "one-way nesting" in RCMs provides an additional forcing and makes possible an analysis of reproducibility of RCM simulations, not only on seasonal as the case with GCMs,

but also on instantaneous time scale. The purpose of this study is to examine the partitioning of RCM simulated time-dependent variables and their seasonal averages between their internal variability component and their reproducible component associated with external forcing. Comparison of the magnitudes of the reproducible and internal variability components provides an insight into their relative significance in dynamical downscaling.

It has been noted in several studies that the large-scale flow in RCMs can systematically deviate from the driving fields, when only forced at the lateral boundary. In order to avoid significant instantaneous large-scale deviations of the RCM variables from the driving fields internal large-scale nudging has been suggested (e.g. von Storch et al., 2000; Biner et al., 2000; Riette and Caya, 2002). In the present study, besides studying the reproducibility of the model solution itself, we perform an analysis of ability of the model to reproduce the large-scale spatial variability of the driving fields in no large-scale nudging case.

The work is organized as follows. In Section 2 the experimental set-up is presented. In Section 3 we examine the spectral behaviour of reproducibility, which provides evidence of how the downscaled information is partitioned between the self-reproducible signal and internal variability at different length scales. The geographical distribution of reproducibility is presented in Section 4. In Section 5 we examine the reproducibility of the seasonal averages. The findings are summarized in Section 6.

2. Experimental setup

2.1 Description of the model

The RCM used in this study is Version 3.6.1 of the Canadian Regional Climate Model (CRCM) initially described in Caya and Laprise (1999). The CRCM is a limited-area grid–point model based on fully elastic non-hydrostatic Euler equations discretized in time by a three-time-level semi-Lagrangian semi-implicit scheme. The physical parameterizations are similar to that described in Caya and Laprise (1999) with exception of the moist convection scheme, which follows the formulation of Bechtold et al. (2001).

In the horizontal, the model performs the computation on a staggered Arakawa C-grid in polar-stereographic coordinates, true at 60°N. The nominal grid-point spacing is 45 km. In the vertical, 18 model levels, defined by a geometric terrain-following Gal-Chen scaled height, were used. The time step used in this experiment was 15 minutes. The nesting technique, developed by Robert and Yakimiw (1986) and Yakimiw and Robert (1990), as proposed by Davies (1976), is based on the relaxation of the horizontal velocity components of the CRCM towards the driving fields in a nine-point wide zone along the lateral boundaries. A complete description of the nesting technique including the dynamical formulation of the CRCM can be found in Laprise et al. (1997).

At the lateral boundaries the CRCM requires information of horizontal velocity, temperature, surface pressure, and specific humidity at each time step. The same set of variables is necessary to define the initial state. In the present study, both the LBC and the IC are derived from the NCEP reanalyses (Kalnay et al., 1996). The LBC are provided by linearly interpolating the 6-hourly NCEP reanalyses on the CRCM grid at each time step.

The set of prognostic variables in the CRCM includes surface variables such as surface temperature, liquid and frozen soil water fraction, and amount and age of snow. These fields

are initialized by their climatological values, while the ocean-surface variables are prescribed from AMIP data.

2.2 Ensemble of simulations

An ensemble of 20 CRCM simulations was generated from May to the end of August 1993 over a domain of *121x121* grid-points covering the east of North America and west of the North Atlantic Ocean (Fig. 1). All the simulations were driven by the same LBC and ocean surface data. The simulations were launched 24 hours apart, starting 1st May 1993 at 0000UTC; thus the last member of the ensemble started on the 20th May 1993 at 0000UTC. The three-month period June-August 1993 is analysed. The spin-up period hence varies from 11 to 30 days. A detailed description of this ensemble may be found in Alexandru et al. (2007).

The domain of analysis consists of 101x101 grid points, exclusive of the 9-point relaxation zone, covering the internal domain area shown in Fig. 1.

3. Analysis of reproducible and irreproducible components of simulated spatial variance

3.1 Definition of reproducible and irreproducible components of model simulations

Let us denote with $X=X_{ijkmn}$ the n^{th} realization of a variable X within an ensemble of N simulations (N=20 here), defined on a rectangular horizontal grid (i,j) with I-by-I computational points ($I=101$ here), at level k in vertical and sampled at times $t_0+m\Delta t$, $m=\{1,2,\ldots,M\}$ ($M=369$ here because fields are sampled every $\Delta t=6hrs$ during the 3 summer months) and t_0 is the 1st June at 0000UTC.

The externally forced, reproducible part of variable X is obtained by the ensemble average defined as

$$\langle X \rangle_{ijkm} = \frac{1}{N} \sum_{n=1}^{N} X_{ijkmn} . \tag{1}$$

Deviations from the ensemble average, defined as

$$X^*_{ijkmn} = X_{ijkmn} - \langle X \rangle_{ijkm} , \tag{2}$$

sample the part of variable X affected by internal variability. Their statistics can be summarized by the standard deviation

$$\varepsilon_{ijkm}(X) \equiv \left\langle X^{*2} \right\rangle^{1/2}_{ijkm} . \tag{3}$$

Fig. 2a shows specific realizations of geopotential height at 925 hPa on 1993.07.25 at 0000UTC. The black, red and blue lines represent three realizations selected from the 20-member ensemble. The ensemble mean computed from all the 20 members of the ensemble is shown in Fig. 2b. The reproducible component of the mass field is devoid of fine-scale details that characterized each of the three realizations shown in Fig. 2a, which indicates the

non-reproducible nature of these features. Fig. 2c shows the standard deviation of the ensemble and NCEP reanalysis utilized to nest and initialize the model are presented in Fig. 2d. For the situation analyzed here, there is very little fine-scale information of the individual CRCM realizations that has survived the ensemble averaging. It is also worth noting that considerable differences are present between the ensemble average and NCEP reanalysis of geopotential height. For example, NCEP fields develop a stronger high over Quebec than the simulated fields, and somewhat weaker Labrador low, while the trough over the Atlantic coast is narrower in NCEP reanalysis.

We now turn our attention to relative vorticity, a field with much more spatial variability at fine scales than geopotential height. Relative vorticity at 925 hPa is shown in Fig. 3 for the three selected realizations of geopotential height shown in Fig. 2a. In the case of vorticity, the ensemble average retains an important amount of small-scale variability. For example the filament of positive vorticity over Labrador associated with the cold front is well preserved, as well as the maximum over the southeastern United States. This is much less the case over Atlantic, where spatial variability is lost in the ensemble average. Unlike the case for geopotential height, the CRCM ensemble average vorticity (Fig. 3b) does add information on fine scales to the NCEP driving fields (Fig. 3d). This implies that, for instantaneous relative vorticity a considerable part of fine-scale variability is generated in reproducible form. For example, the local maximum of vorticity over the Great lakes that can be associated with the warm front (see Fig. 2a) appears almost completely reproducible, as its intensity is not much reduced in the ensemble mean and standard deviation of the ensemble is small (Fig. 3c). Comparison of the standard deviation computed for geopotential height (Fig. 2c) and vorticity (Fig. 3c) shows that locally ensemble spread in one simulated variable does not necessarily implies the spread in other variables, as there is significant spread in geopotential height but little spread in vorticity associated with the warm front over the Great lakes.

Fig. 4 illustrates the decomposition of geopotential height at 925 hPa on 1993.06.20 at 0000UTC. From Fig. 4a it can be inferred that there are little noticeable large-scale differences among the members of the ensemble (now all 20 realizations are shown). Some small-scale differences are nevertheless still present. The most notable small-scale

differences occur over the continental area. It is worth noting that the Midwest low-pressure system combined with a strong ridge over the southeastern US are responsible for the advection of moist air over the large part of the continental area of the domain. The intense convection connected with such a situation might have triggered these small-scale differences, as suggested by Alexandru et al. (2007). Another area of small-scale differences is situated along the frontal zone associated with the trough of the Labrador low. These features are not noticeable in the reproducible part, i.e. the ensemble mean (Fig. 4b), but can be found as weak maxima of the standard deviation of the ensemble shown in Fig. 4c, indicating their irreproducible nature. Additionally, comparison of the CRCM simulated and NCEP-analyzed fields shows considerable discrepancies, as the large-scale low-pressure system observed over Atlantic is absent from all the realizations of the CRCM ensemble.

The corresponding relative vorticity is shown in Fig. 5. Comparison with NCEP reanalyses (Fig. 5d) shows that the model does add the meso-scale spatial variability to the coarse-resolution driving fields. Further, as there is little spread among the CRCM members, most fine-scale features are well preserved in the ensemble average (Fig. 5b), which implies that at this time the CRCM adds value in reproducible form.

3.2 Power spectra of reproducible and irreproducible components

Power spectra of the ensemble average and ensemble deviations can be used to objectively assess the partitioning of downscaled spatial variability between the externally forced, reproducible part and the stochastically variable, non-reproducible component at specified length scales. The separation of scales is performed here utilizing two-dimensional Discrete Cosine Transform (DCT), introduced in analysis of meteorological fields by Denis et al. (2002). A short description of the procedure is given in Appendix A.

The two-dimensional power spectrum of a field X at a fixed level k can be expressed as a scalar function, $S_{qkmn}(X)$, of non-dimensional scalar wave number q, such that $q \in \{1,2,\ldots,(I-1)/2\}$, I denotes the number of computational points along one side of the domain of analysis

($I=101$ here), and m and n denote the sampling time and the realization of the ensemble, respectively. The scalar wavelength that corresponds to wave number q can be computed as

$$l_q = \frac{(I-1)\Delta}{q}, \tag{4}$$

where Δ is the grid spacing assumed to be exactly equal to 45 km, although in reality the grid size varies slightly with latitude in polar-stereographic projection. Therefore, the largest resolved wavelength is 4500 km, while the Nyquist wavelength is 90 km.

Noting by $S_{qkmn}(X)$ the spectral variance at wavenumber q, at level k and at sampling time m, of the n^{th} realization of the CRCM field X, three power spectra can be defined:

$$S^A_{qkm}(X) \equiv \left\langle S_{qkmn}(X) \right\rangle, \tag{5}$$

$$S^R_{qkm}(X) \equiv S_{qkm}\left(\langle X \rangle\right), \tag{6}$$

$$S^I_{qkm}(X) \equiv \left\langle S_{qkmn}\left(X^*\right) \right\rangle. \tag{7}$$

Here S^A represents the ensemble average of the power spectra of the $M=20$ members of field X in CRCM simulations. It can be interpreted as the average power generated by individual realizations. Quantity S^R is the power spectrum of the ensemble average. Quantity S^I is the ensemble average of the power spectra of the individual members' deviation from the ensemble average. It can be shown that the three spectra satisfy the relation (see Appendix B):

$$S^A_{qkm} = S^R_{qkm} + S^I_{qkm}, \tag{8}$$

Hence the average power spectrum S^A is decomposed into S^R - the power spectrum of the reproducible component associated to the external forcing and identifiable with the ensemble average and S^I - the power spectrum of the internal variability component of the model solution about the ensemble average.

The three power spectra computed for the ensemble of realizations of geopotential height on 1993.07.25 at 0000UTC (shown in physical space in Fig. 2), are shown in Fig. 6a. This corresponds to the situation characterized by large spread of simulations. The spectra S^A, S^R, and S^I are presented with the full, dashed and dotted line, respectively. It can be seen that the large scales are dominated by the reproducible component S^R. The irreproducible (internal variability) component S^I increases from length scales of 1500 km to 500 km and dominates at length scales smaller than 500 km.

Also shown in Fig. 6a is the power spectrum of NCEP reanalyses interpolated on the CRCM grid (the red line). The notable decrease in its power at around 1000 km indicates the effective resolution of NCEP reanalyses used to initialize and nest the CRCM simulations. The power does not drop to zero, as might be expected, because the interpolation on the CRCM grid and aliasing in the DCT contaminate the spectrum with some noise. It is worth noting however that this noise has less power than the reproducible component of the C RCM simulations. This means that the ensemble average does contain some added variance at small scales.

Fig. 6b, 6c, and 6d show the decomposed power spectra of relative vorticity (discussed earlier in relation to Fig. 3), divergence and precipitation at the same instant. Relative vorticity and divergence have much more variability at intermediate and small-scale range, i.e. their spectra are much less steep. Thus, at small scales, difference between simulated power and that of regridding noise present in the NCEP curve shows the RCM ability to add value at scales finer than the resolution of the driving data.

When relative vorticity is considered (Fig. 6b), the CRCM added value in the irreproducible component starts to be non-negligible at length scales of 1200km. At 650 km internal variability and reproducible components are equal. Beyond 650km-scale, internal variability dominates. The power spectrum of divergence (Fig. 6c) reveals that internal variability is confined to length scales smaller than 300 km. For precipitation (Fig. 6d), the crossover occurs at even shorter length scales around 200 km.

Fig. 7 shows a similar decomposition of the spectral variance for the situation of 1993.06.20 at 0000UTC characterized by low ensemble spread, examined earlier in Fig. 5. The point of intersection of the power spectra of the reproducible and internal variability components for geopotential height now lies at length scales of approximately 300 km. Relative vorticity (Fig. 7b) exhibits very distinct spectral behaviour with almost its entire power spectrum contained in the reproducible component. For divergence (Fig. 7c) and precipitation (Fig. 7d), the internal variability becomes non-negligible at scales smaller than 300 km.

The two examples examined in this section illustrate that relative contributions of the reproducible and the internal variability components of the model solution can vary substantially during the integration period depending on the simulated weather pattern. In the following we examine the time evolution of their contributions.

3.3 Time series of reproducibility ratio

Reproducibility ratio is defined as follows:

$$\rho_{qkm}(X) \equiv 1 - \frac{S^{I}_{qkm}(X)}{S^{A}_{qkm}(X)}, \tag{9}$$

where q is the wavenumber and k the level and m denotes the sampling time. This ratio takes values between 0 and 1: it approaches 1 when the members of the ensemble are very similar, i.e. the simulations are dominated by the reproducible component and internal variability is small, and approaches 0 when the irreproducible component dominates.

Time series of reproducibility ratio for geopotential height, vorticity and divergence at 925, 500 and 250 hPa, as well as precipitation, are shown in Fig. 8 (in percentage). Five length scales are selected: 2250, 900, 450, 225 and 100 km. In order to make graphs more readable, the daily average of the reproducibility ratio is shown. Large time variations of the reproducibility ratio are present, and they occur in all variables displayed in Fig. 8. In general

the reproducibility ratio increases with length scales and height. The variation of reproducibility ratio with length scale differs greatly between variables. There is a sharp drop in reproducibility ratio for geopotential height around 450 km (Fig. 8a) while it is gradual for other variables. Vorticity is the variable that exhibits the largest reproducibility ratio at the shortest length scale compared to other variables.

Small-scale divergence reproducibility ratio (Fig. 8c) is quite a bit smaller than that of vorticity (Fig. 8b) and precipitation reproducibility ratio (Fig. 8d) closely follows that of divergence. For example, at 100 km, it is most of time below 40 % at all levels. This may be a fingerprint of convection that dominates small-scale precipitation in summer and is associated with the divergent component of the flow.

It is important to note that Fig. 8 provides no evidence that the reproducibility ratio of fine-scale surface variables is considerably higher than that aloft as might be expected if surface forcing played a dominant role. It should be noted however that the domain of this study is characterized with modest topography and the ocean covers a large part of the domain.

The representative reproducibility ratio of a time-dependent instantaneous CRCM variable X for the entire integration period is computed as follows:

$$\rho_{qk}(X) \equiv 1 - \frac{\overline{S_{qk}^{I}}(X)}{\overline{S_{qk}^{A}}(X)} = \frac{\overline{S_{qk}^{R}}(X)}{\overline{S_{qk}^{A}}(X)}, \tag{10}$$

where the over-bar denotes the time-average

$$\overline{(\ )} \equiv \frac{1}{M}\sum_{m=1}^{M}(\ ). \tag{11}$$

It is worth mentioning that definitions of time average ρ_{qk} distinct form (10) are possible, but this particular one is chosen since it satisfies the equality on the rhs of (10).

Fig. 9 shows the distribution of ρ_{qk} as a function of height and horizontal length scale. Values of ρ_{qk} are noticeably larger for vorticity (Fig. 9b) at all levels. At scales smaller than 200 km, geopotential height (Fig. 9a) and divergence (Fig. 9c) exhibit very small ρ_{qk}. Nevertheless, the absence of significant vertical gradient of reproducibility ratio near the surface (except in vorticity between 200 and 100 km) suggests that surface forcing, in our integrations, does not exert a strong control to reduce internal variability.

In Fig. 10 shows, the time-average spectral variances $\overline{S^A}$, $\overline{S^R}$, and $\overline{S^I}$, computed as the time-average of Equations (5)-(7). For geopotential height the reproducible component of the spectral variance dominates for scales larger than approximately 300 km while the variable component dominates at smaller scales. For precipitation and low-level divergence, the crossover occurs at length scale of 150 km. Vorticity on the other hand is dominated by the reproducible component at all length scales.

It should be noted in Fig. 10 that the variances of NCEP reanalyses and the ensemble-average power spectrum of the CRCM members, $\overline{S^A}$, are not identical at large scales, indicating that the simulated large-scale spatial variability of various variables deviates systematically from that of the driving fields. For example, it can be seen in Fig. 10b that, in the range of large scales, the ensemble-average time-average power spectrum $\overline{S^A}$ of vorticity (full line) is larger than NCEP power spectrum (red line) at 925 hPa. However, it is smaller than NCEP spectrum at 250 hPa. The same can be seen for geopotential height (Fig. 10a). We will study this in detail in the next subsection.

3.4 Deviation of amplitudes of CRCM simulation with respect to NCEP reanalyses

In order to examine the capability of the model to reproduce large-scale variance of the driving fields the accrued amplitude of CRCM simulations with respect to NCEP reanalyses is defined as follows:

$$\eta_{qk}(X) \equiv 1 - \frac{\overline{S^D_{qk}(X)}}{\overline{S^A_{qk}(X)}}. \tag{12}$$

Here S^D and S^A denote the power spectrum of driving NCEP reanalyses and the average power generated by individual realizations of the ensemble as given by Equation (5), respectively. The over-bar denotes the time average. At scales resolved by the coarse-resolution driving fields that are provided at the lateral boundaries, the optimal value of the coefficient η_{qk} is 0. This is the case if the power of the driving fields and the average power of the simulated fields are identical. At scales finer than those resolved by the driving fields, the optimal value is 1, as at this range of the spectrum S^D represents no more than regridding noise and aliasing in the DCT. Further, η_{qk} takes positive (negative) values when the average members power is larger (smaller) than that of the driving fields. Note that $\eta_{qk} \leq 1$.

The accrued variance η_{qk} is computed for geopotential height, relative vorticity and divergence, and shown in percent in Fig. 11 as a function of length scale and height. It can be seen that the amplitudes of the large-scale geopotential height, in CRCM simulations are overestimated near the surface and underestimated at higher levels. The simulated relative vorticity (Fig. 11b) exhibits similar excess at large scales in the low levels and amplitude deficiency above 750 hPa. On the other hand the power of the simulated large-scale divergence (Fig. 11c) is underestimated at all pressure levels, compared to NCEP reanalyses.

Time series of accrued variance coefficient, defined as

$$\eta_{qkm}(X) \equiv 1 - \frac{S^D_{qkm}(X)}{S^A_{qkm}(X)}, \tag{13}$$

computed for geopotential height at 925, 500 and 250 hPa at three largest wavelengths of 4500, 2250 and 1125 km, are shown in Fig. 12 (in percent). The accrued variance varies considerably in time, especially at 1125 km (red line) at high levels (Fig. 12b,c). The negative bias of the geopotential height spatial variance at high levels at 1125 km scale, seen in Fig. 11a, is due to episodes of strong underestimation that occur frequently and leave the fingerprint in the average accrued variance shown in Fig. 11a. At 500 and 250 hPa,

underestimation as low as –250% is noted, indicating that average members variance S^A is then 3.5 times smaller than NCEP-analyzed variance S^D. However, near the surface (Fig. 12a), although the geopotential height CRCM large-scale spatial variance is intermittently strongly underestimated, the average bias is positive.

It is worth mentioning that the accrued variance coefficient (Fig. 12) does not exhibit a tendency in time. There is also no considerable correlation between the accrued variance coefficient and reproducibility ratio (not shown).

4. Analysis of reproducible and irreproducible components of transient eddy variance

The method employed in the previous section focused on the analysis of reproducibility of spatial variability. Here we examine the capability of the ensemble average to provide valuable information on temporal evolution of the simulated variables at a given grid point. This is done by the separation of the temporal variance, that is function of space, in the reproducible and variable components.

4.1 Definition of reproducible and irreproducible components of the transient-eddy variance

The transient-eddy variance of individual realizations of field X_{ijkmn} is computed by

$$\sigma^2_{ijkn}(X) \equiv \overline{\left(X_{ijkmn} - \overline{X}_{ijkn}\right)^2}, \tag{14}$$

with *(i,j)* the horizontal grid index, k the level index, m the sampling time and n is the member in the ensemble for variable X. Here the over-bar denotes the time average on m for a season. The ensemble average of the transient-eddy variance is defined as

$$\sigma^{2\,A}_{ijk}(X) = \left\langle \sigma^2_{ijkn}(X) \right\rangle, \tag{15}$$

and it can be decomposed as

$$\sigma^{2\,A}_{ijk} = \sigma^{2\,R}_{ijk} + \sigma^{2\,I}_{ijk}, \tag{16}$$

where

$$\sigma^{2\,R}_{ijk}(X) = \sigma^2_{ijk}\left(\langle X \rangle\right), \tag{17}$$

$$\sigma^{2\,I}_{ijk}(X) = \left\langle \sigma^2_{ijkn}\left(X^*\right) \right\rangle. \tag{18}$$

Here, $\sigma_{ijk}^{2\ R}$ represents the transient-eddy variance of the ensemble mean (the reproducible component of the ensemble), and $\sigma_{ijk}^{2\ I}$ corresponds to the ensemble-mean transient-eddy variance of the irreproducible component of the ensemble. In Appendix C it is shown that the time-average variance of members about the ensemble mean (3), the standard measure of spread among the simulations in studies of internal variability, can be decomposed into the sum of $\sigma_{ijk}^{2\ I}$ and a contribution from the inter-member variance of the time mean. In Alexandru et al. (2007) it can be seen that the inter-member variance of seasonal averages is much smaller than the seasonally averaged inter-member variance. Thus, the irreproducible component of the transient-eddy variance is approximately equal to the time average inter-member variance of the ensemble: this is a special form of the ergodicity property.

Prior to computing the various transient-eddy variances, the CRCM-simulated fields are separated in their horizontal large-scale and small-scale components. This is done because the large-scale components of model variables are not significantly affected by internal variability. At the scale of the regional domain of this study, most of the atmospheric variables have negative spectral slopes, implying that the large part of their spatiotemporal variability is confined to large scales. Thus, without separation of large-scales, internal variability at fine scales would be unnoticeable because of high reproducibility of large scales.

The separation of scales is performed using the DCT (Denis et al., 2002). A low-pass (high-pass) filter is defined such that it preserves (removes) all amplitudes at scales larger than 1200 km and removes (preserves) all amplitudes at scales smaller than 800 km. The resulting two components of simulated fields are denoted as the large-scale and the small-scale part. The filter is defined in order to mimic the effective resolution of the driving fields. As it was shown earlier, the effective resolution of regridded NCEP reanalyses is approximately 1000 km (e.g. Fig. 6).

Fig. 13 shows the decomposition for geopotential height at 925 hPa of the ensemble average of transient-eddy variance $\sigma_{ijk}^{2\ A}$ in the reproducible $\sigma_{ijk}^{2\ R}$ and irreproducible part σ_{ijk}^{2I}. Note that square roots of the variances (transient-eddy standard deviations) are shown instead of variances. For large scales the reproducible part (Fig. 13a) of transient-eddy variability is

much larger than the irreproducible part (Fig. 13b). This is very different from the situation with GCM, as a result of the control exerted by LBC in the nested models. For small-scales, however, the irreproducible component (Fig. 13d) can locally contribute more to the transient-eddy amplitudes than the reproducible component, such as over regions of the Gulf Stream (Fig. 13c).

Geographical distribution of the reproducibility ratio can now be assessed with the coefficient

$$\rho_{ijk}(X) \equiv 1 - \frac{\sigma_{ijk}^{2\,I}(X)}{\sigma_{ijk}^{2\,A}(X)}. \tag{19}$$

We examine reproducibility ratio of large and small scales separately in the next two subsections. It is worth noting that in autonomous global models, beyond their predictability limit, this index vanishes.

4.2 Reproducibility ratio of large scales

Fig. 14, 15, and 16 show, in percentage, the reproducibility ratio of large-scale components of vorticity, divergence and precipitation at selected pressure levels. Reproducibility ratio of large scales is, in general, high, especially near the perimeter of the domain because of the control exerted by the LBC, especially on the inflow side, over the west and the northwest part of the domain. This pattern of reproducibility ratio is preserved at all heights with a shift of the minimum at 500 and 250 hPa, although the values differ. The lowest reproducibility ratio of large-scale components of the CRCM fields is found near the ground.

Fig. 14 shows that transient eddies of large-scale vorticity are almost completely reproducible at the northwest part of the domain due to inflow side of the domain. The reproducibility ratio is significantly lower, especially over the ocean, where it drops as low as to 85 %. Reproducibility ratio of large-scale divergence (Fig. 15) has a very similar geographical distribution to that of relative vorticity with slightly higher values and

maximum in the mid-troposphere. Large-scale precipitation, shown in Fig. 16, mainly follows the pattern and magnitude of the reproducibility ratio of large-scale vorticity at 925 hPa (Fig. 15a). It is worth noting that reproducibility ratio is a relative quantity; therefore, the minimum reproducibility ratio of 84 % over the northwest Atlantic Ocean does not necessarily coincides with largest ensemble spread in absolute values of precipitation. The maximum spread in 6-hourly precipitation (not shown) occurs over the Mississippi Delta and is marked with the local minimum of reproducibility ratio of large-scale precipitation in this area (Fig. 16). The reproducibility ratio of transient eddies of large-scale geopotential height has a similar geographical distribution but values are considerably higher and does not drop below 98 % (not shown).

We note that the model variables exhibit decreased reproducibility ratio of their large-scale components near the surface. Thus presence of surface forcing and topography, in general, does not appear to reduce the internal variability at large scales. The control the lateral boundary conditions exert on the evolution of the RCM simulation by advection of information from the lateral boundaries towards the interior of the domain decreases with increasing residence time. The reproducibility of large scales at low levels may be smaller due to weaker average wind speed and increased residence time of air parcels within the domain.

4.3 Reproducibility ratio of small scales

Inspection of geographical distribution of reproducibility ratio of small scales (Fig. 17-20) shows patterns similar to those of large scales but with smaller values. This is the consequence of the fact that even a slight temporal decorrelation between large-scale features simulated by two members of the ensemble will cause a strong temporal decorrelation of embedded small-scale features (de Elía et al., 2002). Although strongly influenced by large scales, geographical distribution of reproducibility ratio of small-scale components exhibits their specific features. In the south of the continent, where the reproducibility ratio of large scales is relatively high when compared to that in other regions, the reproducibility ratio of small scales is very low. This shows that it could be more sensitive to variable, surface type,

topography and role that convective processes and hydrodynamic instabilities play in local climate than the reproducibility ratio of large scales.

Reproducibility ratio of transient-eddy small-scale geopotential height is shown in Fig. 17. In the northwest part of the domain the reproducibility ratio is very high, ranging from 90 to 100 % at all levels. The reproducibility ratio decreases quickly toward the south. For example, at 925 hPa the reproducibility ratio as low as 20-40 % can be seen over a large part of the continent, from the Gulf of Mexico to the Great Lakes (Fig. 17a). Particularly, just south of the Great Lakes basin, there is a strong minimum in reproducibility ratio, which is not associated with a low reproducibility ratio of large scales of other variables (Fig. 14-16).

Over the continent the reproducibility ratio generally decreases with height (except at upper levels), which is less notable over the ocean. Fig. 17e shows the vertical cross section along the arrow denoted in Fig. 17a. It can be seen that vertical distribution of reproducibility ratio of small-scale geopotential height over the continent is very distinct from that over the ocean. Over the continent the reproducibility ratio minimum occurs at levels between 700 and 500 hPa, while over the ocean it occurs at levels immediate to the surface. The strong convection over the relatively warm continental surface might be responsible for this feature.

The pattern of reproducibility ratio of transient-eddy small-scale geopotential height over the ocean at lower levels is characterized with long and narrow areas of very low values: these appear to be fingerprints of trajectories of specific weather events giving rise to large ensemble spread. Such episodes are documented in Alexandru et al. (2007).

Reproducibility ratio of transient-eddy variance of small-scale relative vorticity is shown in Fig. 18. One can see that areas in the northwest and west part of the domain (the Great Lakes and Hudson Bay) are characterized with values even higher then 90 %. The values decrease eastward and southward. The reproducibility ratio of small-scale vorticity follows the geographical distribution of the reproducibility of its large scales: the minimum is situated in the southeast United States and extends over the large part of northwest Atlantic Ocean. It also increases with height; for example, at 250 hPa, it is larger then 60 % everywhere in the domain.

Reproducibility ratio of small-scale divergence is shown in Fig. 19. The highest values are again found in the far northwest and southeast part of the domain, but they are smaller and hardly exceed 90 %. Reproducibility ratio of small-scale divergence is somewhat higher over the Grate Lakes and along the Appalachians and takes values from 80-90 %. The area of minimum extends from the southeastern United States toward the northeast over the ocean with values ranging from 30-60 %.

This small-scale component of divergence does not appear to be strongly linked to the corresponding large-scale component, unlike the case for relative vorticity. Firstly, the reproducibility of small-scale divergence is considerably smaller than that of small-scale vorticity at all levels. Further, except in Mississippi delta, the small-scale divergence reproducibility ratio over the continent is lower at 700 hPa (Fig. 19b) than near the surface (Fig. 19a), which was not the case for small-scale vorticity, (see Fig. 18a and 18b). This might be due to the fact that small-scale disturbances of relative vorticity are frequently embedded in synoptic low-pressure systems, where they appear as filaments associated with meso-scale phenomena as fronts and thunderstorm lines. On the contrary, small-scale divergence is more associated with convection.

Reproducibility ratio of small-scale precipitation is shown in Fig. 20. It is very similar to that of low-level small-scale divergence (Fig. 19a). The highest values of 80-95 % characterize the northwest part of the domain. In the rest of the domain, the reproducibility ratio ranges from 30-60 %.

5. Analysis of reproducible and irreproducible components of seasonal averages

We now turn our attention to seasonally averaged fields, which may also be called stationary-eddy component. These are again decomposed into reproducible, ensemble-mean and variable, irreproducible components, as well as scale-decomposed with the DCT. The ensemble-average stationary-eddy variance S^A and its reproducible S^R and irreproducible components S^I, are computed using Equations (4), (5) and (6), for the seasonally averaged quantities rather than instantaneous variables as was done in Section 3.

Fig. 21 shows the spatial power spectra of these quantities for seasonal-average CRCM-simulated geopotential height, relative vorticity, divergence and precipitation, as well as the power spectra of the corresponding NCEP reanalyses. For all seasonally averaged fields, the reproducible component (dashed line) dominates over the irreproducible component (dotted line) in the entire spectrum. However the magnitude of the irreproducible component becomes non-negligible at scales smaller than *200km*.

In case of vorticity (Fig. 21b) and divergence (Fig. 21c), the ensemble-average of the members' power spectra S^A (full line) is much larger than the power spectrum of driving NCEP fields (red line) at scales smaller than 1000 km, that, as mentioned earlier, indicates the effective resolution of the driving fields. This shows the ability of the CRCM to add an important amount of fine-scale variance in seasonal climate statistics, but the generated fine-scale information is only partly reproducible.

The reproducibility ratio of seasonal-average variables is shown in Fig. 22. Unlike the case for instantaneous variables, seasonal averages exhibit important variations of the reproducibility ratio with height. In general, near surface the fields have larger reproducibility ratio at small scales than aloft. This is especially noticeable for vorticity and divergence. Reproducibility ratio of precipitation (not shown) drops near 70 % at scales smaller than 200 km.

6. Concluding remarks

The purpose of this work was to identify the components of the fields simulated by nested, limited-area models that are controlled by the boundary conditions in a deterministic sense (referred to as reproducible components) and those that are, in this sense, free and thus variable or irreproducible. In this study, a 20-member ensemble of integrations of the CRCM, driven by NCEP reanalyses, is conducted for a summer season over a mid-latitude domain. Model-simulated variables and their seasonal averages are decomposed in a reproducible signal, defined as the ensemble mean, and an irreproducible component resulting from deviations about the ensemble mean. The partition of the model solution between these two components as function of length scale, geographical position within the domain, height and weather episodes during the season is examined.

The results show that internal variability is scale-selective, the smallest scales being the most affected. Large-scale flow is rather strongly controlled by boundary conditions, although it is intermittently affected with important spread among members in the ensemble. The high reproducibility of large scales is present in all variables and exhibits a minimum at low levels. This might be associated with increased residence time of near-surface air parcels in the interior of the domain. On the other hand, the reproducibility ratio of small scales is slightly increased near the surface, which can be attributed to the surface forcing.

Large-scale transient eddies of all variables exhibit the same spatial pattern of reproducibility: they are completely reproducible at the inflow boundaries and the internal variability component increases downstream. The geographical distribution of reproducibility of small scales mainly follows the pattern of large scales, but the values are considerably smaller. Similarly, the temporal pattern of reproducibility of small-scale components is relatively well synchronized with that of reproducibility of large scales. This is especially the case for relative vorticity for which the reproducibility ratios of large and small scales appear to be tightly linked. On the other hand, reproducibility of small-scale components of mass

field has additional minima situated over the warm continental surface, in areas where reproducibility of its large-scale components is very high. This might be associated with convection.

The fact that spatiotemporal variations of the reproducibility ratio of large and small scales are linked implies that increased reproducibility of large scales is likely to increase reproducibility of small scales. The large-scale nudging (e.g. von Storch *et al.*, 2000; Biner *et al.*, 2000; Riette and Caya, 2002) has been applied in RCM simulations in order to force the simulated large-scale circulation towards that prescribed by driving fields. It might improve the reproducibility of fine scales in RCM simulations, however it could diminish the ability of the model to add value in the small-scale range. These two hypotheses have not been investigated further in this study.

Comparison of the power spectra of the CRCM and NCEP analyzed time-dependent variables shows that, in an instantaneous sense, the CRCM generated a considerable amount of fine-scale variability, despite the fact that it was nested and initialized with data that contained large scales only. It is worth noting that this holds as well for the noisy quantities with flatter spectra are considered. Such variables have a large part of their spatial variance distributed at fine scales, because their variability is associated with fine-scale features such as fronts and thunderstorm lines or convective cells. It is necessary for an RCM to be capable of simulating such meso-scale phenomena in order to provide realistic information on local climate. Our results support an optimistic point of view regarding this issue. Furthermore, the scale analysis of CRCM and NCEP seasonal averages reveals that the CRCM-added information on fine-scale variability of the seasonal climate.

The value added by RCM simulations is considerably affected by internal variability. For instantaneous variables, the irreproducible component dominates the reproducible component at fine scales. When reproducibility of seasonal averages is examined, the results show that, although largely filtered from the model solution, the irreproducible component is non-negligible at fine scales. Near the surface all CRCM variables have their fine scales highly reproducible. However, at upper levels and at scales smaller than 200 km the internal

variability component becomes not negligible, which reflects in the relatively low reproducibility ratio of seasonal precipitation at those scales.

Comparison of the large-scale spatial variance of the CRCM and NCEP driving fields for time-dependent variables revealed that spatial variance of CRCM surface variables is, on average, slightly overestimated near the surface, and considerably underestimated in the upper troposphere. The reasons for this are still under investigation. Large-scale nudging in RCM simulations would prevent such differences in RCM simulations.

Acknowledgments

This research was done as a project within the Canadian Network for Regional Climate Modelling (CRCM) and the Canadian Network on Climate Variability (CLIVAR), funded by the Canadian Foundation for Climate and Atmospheric Sciences (CFCAS), the National Science and Engineering Research Council (NSERC) and the Ouranos Consortium on Regional Climatology and Adaptation to Climate Change.

APPENDIX A: Discrete Cosine Transform (DCT)

The DCT is employed to compute power spectra of simulated fields, because it has been shown appropriate for fields having spectral slopes within a relatively wide range between –4 and +1, which encompasses the most atmospheric fields. The spectral slopes of ensemble averages and ensemble deviations also fall within this range, which approves the employment of the DCT in this study. The DCT procedure is entirely equivalent to the Discrete Fourier Transform (DFT), except that it includes pre-processing of fields, based on one mirror reflection along the two opposite lateral boundaries. The effect of the pre-processing is a considerable decrease of the erroneous effect of the boundary discontinuities. With the mirror reflection fields become even, thus cancelling projections on Fourier sine modes.

Let us assume that $X=X_{ij}$ be the field defined on a horizontal grid (i,j) of I-times-I computational nods. The direct DCT of X is given by

$$\Psi_{\lambda\mu}(X) = \beta_\lambda \beta_\mu \sum_{i=0}^{I-1}\sum_{j=0}^{I-1} X_{ij} \cdot \cos\left[\pi\lambda\frac{i+1/2}{I}\right]\cdot\cos\left[\pi\mu\frac{j+1/2}{I}\right], \tag{A1}$$

and the inverse DCT is given by

$$X_{ij} = \sum_{\lambda=0}^{I-1}\sum_{\mu=0}^{I-1} \beta_\lambda \beta_\mu \Psi_{\lambda\mu}(X) \cdot \cos\left[\pi\lambda\frac{i+1/2}{I}\right]\cdot\cos\left[\pi\mu\frac{j+1/2}{I}\right], \tag{A2}$$

where $\lambda,\mu\in\{0,1,2,\ldots,I\text{-}1\}$ and

$$\beta_s = \begin{cases} \sqrt{1/I} & s=0 \\ \sqrt{2/I} & s=1,2,\ldots,I-1 \end{cases} \tag{A3}$$

for $s=\lambda,\mu$. Here, λ is the x and μ the y non-dimensional wave number. In order to express the variance as a function of spatial scale only, a scalar wave number

$$\vartheta = \sqrt{\lambda^2 + \mu^2} \tag{A4}$$

is defined and power that correspond to all scalar wave numbers within the interval $(q-1/2,q+1/2)$ for $q \in \{1,2,\ldots,(I-1)/2\}$ are then gathered. The power that corresponds to length scales outside of the circle drawn at the Nyquist scalar wave number

$$\vartheta = (I-1)/2 \tag{A5}$$

is omitted. Thus. the DCT of X can be expressed as a function of length scale:

$$l_q = \frac{(I-1)\Delta}{q}, \tag{A6}$$

where Δ is the grid-spacing (*45km* here), and it can be denoted as $\Psi_q(X)$..

Because projections on sine modes are absent in the DCT, the power spectrum of a variable X is given as

$$S_q(X) = \Psi_q^2(X). \tag{A7}$$

APPENDIX B: Decomposition of power spectra in reproducible and irreproducible components

Let us assume $X=X_{ijn}$ as the n^{th} realization of a simulated 2D field within an ensemble of N simulations, on I-by-I computational points of a discrete horizontal grid (i,j). The ensemble average is defined as

$$\langle X \rangle_{ij} \equiv \frac{1}{N} \sum_{n=1}^{N} X_{ijn} . \tag{B1}$$

Then the field X can be decomposed as

$$X = \langle X \rangle + \left(X - \langle X \rangle \right). \tag{B2}$$

Upon substituting Equation (B2) in Equation (A1) of the Appendix A, it is straightforward to show that the discrete cosine transform of X_{ijn} denoted as $\Psi_{qn}(X)$, satisfy the relationship:

$$\Psi_{qn}(X) = \Psi_q\left(\langle X \rangle\right) + \Psi_{qn}\left(X - \langle X \rangle\right). \tag{B3}$$

Here q denotes the wave number as defined in Appendix A. Upon squaring Equation (B3) and taking account of Equation (A7) of Appendix A, the power spectrum of X_{ijn}, denoted as S_{qn}, can be expressed as follows:

$$S_{qn}(X) = S_q\left(\langle X \rangle\right) + S_{qn}\left(X - \langle X \rangle\right) + 2 \cdot \Psi_q\left(\langle X \rangle\right) \cdot \Psi_{qn}\left(X - \langle X \rangle\right). \tag{B4}$$

The ensemble average of all power spectra is given by

$$S_q^A(X) = \left\langle S_{qn}(X) \right\rangle, \tag{B5}$$

the reproducible power spectrum is defined as the power spectrum of the ensemble mean, i.e.

$$S_q^R(X) = S_q\left(\langle X \rangle\right), \tag{B6}$$

and the irreproducible power spectrum as the ensemble average of power spectra of individual members deviations from the ensemble average:

$$S_q^I(X) = \left\langle S_{qn}\left(X - \langle X \rangle\right)\right\rangle. \tag{B7}$$

Applying the operator < > on Equation (B4) we obtain:

$$S_q^A(X) = S_q^R(X) + S_q^I(X) + \frac{2}{M} \cdot \Psi_q\left(\langle X \rangle\right) \cdot \left\langle \Psi_{qn}\left(X - \langle X \rangle\right)\right\rangle. \tag{B8}$$

According to the definition of the DCT in Appendix A, the sum in the last term on the rhs of (B8) vanishes, i.e.:

$$\left\langle \Psi_{qn}\left(X - \langle X \rangle\right)\right\rangle \equiv 0. \tag{B9}$$

Therefore, the power spectra S^R and S^I partition the power spectrum S^A:

APPENDIX C: Relation between the irreproducible part of transient-eddy variance and the time-average inter-member variance

Let X_{ijmn} be the n^{th} realization of an ensemble of time dependent variable defined on a horizontal grid (i,j), sampled at times $t_0+m\Delta t$, $m=\{1,2,\ldots,M\}$. The ensemble mean and ensemble deviation are defined as

$$\langle X \rangle_{ijm} \equiv \frac{1}{N}\sum_{n=1}^{N} X_{ijmn}, \tag{C1}$$

$$X^{*}_{ijmn} \equiv X_{ijmn} - \langle X \rangle_{ijm}, \tag{C2}$$

and the time average and the transient eddy as

$$\overline{X}_{ijn} \equiv \frac{1}{M}\sum_{m=1}^{M} X_{ijmn}, \tag{C3}$$

$$X'_{ijmn} \equiv X_{ijmn} - \overline{X}_{ijn}. \tag{C4}$$

Transient-eddy variance of a member X_{ijmn} is defined as

$$\sigma^2_{ijn}(X) = \overline{\left(X'_{ijmn}\right)^2}, \tag{C5}$$

and the time-dependent variance of individual realizations around their ensemble mean (ensemble spread) as

$$\varepsilon^2_{ijm}(X) \equiv \left\langle \left(X^{*}_{ijmn}\right)^2 \right\rangle. \tag{C6}$$

The transient-eddy variance of deviation of the n^{th} realization of X around the ensemble mean can be rewritten in the form

$$\sigma^2_{ijn}(X^*) = \overline{\left(X^*_{ijmn}\right)^2} - \left(\overline{X^*_{ijmn}}\right)^2. \tag{C7}$$

Because the time averaging and the averaging among members in the ensemble are independent, (C7) can be rewritten as follows:

$$\sigma^2_{ijn}(X^*) = \overline{\left(X^*_{ijmn}\right)^2} - \left(\overline{X}^*_{ijn}\right)^2. \tag{C8}$$

Applying the ensemble-average operator (C1) on Equation (C8) we obtain

$$\sigma^{2\,I}_{ij}(X) \equiv \left\langle \sigma^2_{ijn}(X^*) \right\rangle = \overline{\left\langle \left(X^*_{ijmn}\right)^2 \right\rangle} - \left\langle \left(\overline{X}^*_{ijn}\right)^2 \right\rangle, \tag{C9}$$

where $\sigma_{ij}{}^{2\,I}$ represents the irreproducible part of transient-eddy variance, defined in Equation (18). From (C6) and (C9) it follows that:

$$\overline{\varepsilon^2_{ijm}(X)} = \varepsilon^2_{ij}\left(\overline{X}\right) + \sigma^{2\,I}_{ij}(X). \tag{C10}$$

Equation (C10) shows that the time-average inter-member variance is contributed by the inter-member variance of the time averages (stationary eddies) and the variable, non-reproducible component of transient-eddies variance.

REFERENCES

Alexandru A., R. de Elía and R. Laprise, 2007: Internal variability in Regional Climate Downscaling at the seasonal scale. *Mon. Wea. Rev.*, **135**, 3221–3238.

Anthes R. A., Y. H. Kuo, D. P. Baumhefner, R. M. Errico and T. W. Bettge, 1985: Predictability of Mesoscale Atmospheric Motions, Advances Geophys., **288**, Academic Press, 159-202.

Bechtold, P., E. Bazile, F. Guichard, P. Mascart and E. Richard, 2001: A mass flux convection scheme for regional and global models. *Q. J. R. Meteorol. Soc.*, **127**, 869-886.

Biner, S., D. Caya, R. Laprise and L. Spacek, 2000: Nesting of RCMs by imposing large scales, 7.3-7.4. Research activities in Atmospheric and Oceanic Modelling, edited by H.Richie, WMO/TD - No. 987, Report No. **30**. 7.3-7.4

Boer G. J., 1984: A spectral Analysis of Predictability and Error in an Operational Forecast System, Mon. Wea. Rev., **112**, 1183-1197.

Boer G. J., 1993: Systematic and Random Error in an Extended-Range Forecasting Experiment. Mon. Wea. Rev., **121**, 173-188.

Castro, C. L., R. A. Pielke, Sr., and G. Leoncini, 2005: Dynamical Downscaling: An Assessment of Value Added Using a Regional Climate Model, J. Geophys. Res.-Atmospheres **110**, D05108, doi:10.1029/2004JD004721.

Caya D. and S. Biner, 2004: Internal Variability of RCM Simulations Over an Annual Cycle, Clim. Dyn., **22**, 33-46.

Caya D. and R. Laprise, 1999: A semi-implicit semi-Lagrangian regional climate model: the Canadian RCM. Mon. Wea. Rev., **127**, 341-362.

Christensen O. B., M. A. Gaertner, J. A. Prego and J. Polcher, 2001: Internal Variability of Regional Climate Models, Clim. Dyn., **17**, 875-887.

Davies H. C., 1976: Lateral Boundary Formulation for Multi-level Prediction Models, Quart. J. R. Met. Soc., **102**, 405-418.

Davis H. C. and R. E. Turner, 1977: Updating Prediction Models by Dynamical Relaxation: an Examination of the Technique, Quart. J. R. Met. Soc., **103**, 225-245.

De Elía R., R. Laprise and B. Denis, 2002: Forecasting Skill Limits of Nested, Limited-Area Models: A Perfect Model Approach, Mon., Wea. Rev., **130**, 2006-2023.

Denis B., R. Laprise, D. Caya and J. Cote, 2002: Downscaling Ability of One-Way Nested Regional Climate Models: The Big-Brother Experiment, Clim. Dyn., **18**, 627-646.

Denis B., J. Côté and R. Laprise, 2002, Spectral Decomposition of Two-Dimensional Atmospheric Fields on Limited-Area Domains Using the Discrete Cosine Transform (DCT), Mon. Wea. Rev., **130**,1812-1829.

Gates, W. L., 1992: AMIP: The Atmospheric Model Intercomparison Project, Bull. American Meteor. Soc., **73**, (12), 1962-1970.

Giorgi F. and X. Bi, 2000: A Study of Internal Variability of a Regional Climate Model, J. Geophys. Res., **105**, D24, 29503-29521.

Giorgi F. and L. O. Mearns, 1999: Introduction to Special Section: Regional Climate Modelling Revisited, J. Geophys. Res., **104**, D6, 6335-6352.

Jones R. G., J. M. Murphy, M. Noguer and M. Keen, 1997: Simulation of Climate Change over Europe Using a Nested Regional-Climate Model. II: Comparison of Driving and Regional Model Responses to a doubling of Carbon Dioxide, Quart. J. R. Meteorol. Soc., **123**, 265-292.

Kalnay E., M. Kanamitsu, R. Kistler, W. Collins, D. Deaven, L. Gandin, M. Iredell, S. Saha, G. White, J. Woollen, Y. Zhu, A. Leetmaa, B. Reynolds, M. Chelliah, W. Ebisuzaki, W. Higgins, J. Janiwiak, K. C. Mo, C. Ropelewski, J. Wang, R. Jenne and D. Joseph, 1996: The NCEP/NCAR 40-Year Reanalysis Project, Bull. American Meteor. Soc., **77**, (3), 437-471.

Laprise R., D. Caya, D. Bergeron and M Giguère, 1997: The formulation of André Robert MC2 (Mesoscale Compressible Community) model. The André J. Robert Memorial Volume (C. Lin, R. Laprise, and H. Ritchie, Eds.), companion volume to Atmos.-Ocean, **35**, 195-220.

Laprise R., M. R. Varma, B. Denis, D. Caya and I. Zawadzki, 2000: Predictability of a Nested Limited-Area Model, Mon. Wea. Rev., **128**, 4149-4154.

Lorenz, E. N., 1969: The predictability of a flow which possesses many scales of motion. *Tellus*, **21**, 289-307.

Lorenz, E. N., 1982: Atmospheric predictability experiments with a large numerical model. *Telluss*, **34**, 505-513.

Miguez-Macho, G., G. L. Stenchikov and A. Robock, 2004: Spectral nudging to eliminate the effects of domain position and geometry in regional climate simulations, J. Geophys. Res., **109** (D13), D13104, 10.1029/2003JD004495.

Riette, S. and D. Caya, 2002: Sensitivity of short simulations to the various parameters in the new CRCM spectral nudging. Research activities in Atmospheric and Oceanic Modelling, edited by H. Ritchie, WMO/TD - No 1105, Report No. 32: 7.39-7.40.

Rinke, A., P. Marbaix, and K. Dethloff, 2004: Internal Variability in Arctic Regional Climate Simulations: Case Study for the Sheba year, Climate Res., **27**, 197-209.

Robert A. and E. Yakimiw, 1986: Identification and elimination of an inflow boundary computational solution in limited area model integrations, Atmos.-Ocean, **24**, 369-385.

Schubert D. and M. Suarez, 1989: Dynamical Predictability in a Simple General Circulation Model: Average Error Growth, J. Atmos. Sci., **46**, 353-370.

Stern, W., and K. Miyakoda, 1995: Feasibility of Seasonal Forecasts Inferred from Multiple GCM Simulations, J. Clim., **8**, 1071-1085.

Van Tuyl A. H., and R. M. Errico, 1989: Scale Interaction and Predictability in Mesoscale Model, Mon. Wea. Rev., **117**, 495-517.

Von Storch, H., H. Langenberg and F. Feser, 2000: A spectral nudging technique for dynamical downscaling purposes, Mon. Wea. Rev., **128**, 3664-3673.

Vukicevic T. and R. M. Errico, 1990: The Influence of Artificial and Physical Factors upon Predictability Estimates Using a Complex Limited-Area Model, Mon. Wea. Rev., **118**, 1460-1482.

Vukicevic T. and J. Paegle 1989: The Influences of One-Way Interacting Lateral Boundary Conditions upon Predictability of Flow in Bounded Numerical Models, Mon. Wea. Rev., **117**, 340-350.

Weisse R., H. Heyen and H. von Storch, 2000: Sensitivity of a Regional Atmospheric Model to a Sea State-Dependent Roughness and the Need for Ensemble Calculations, Mon. Wea. Rev., **128**, 3631-3643.

Yakimiw E. and A. Robert, 1990: Validation experiments for a nested grid-point regional forecast model, Atmos.-Ocean, **28**, 466-472.

FIGURES

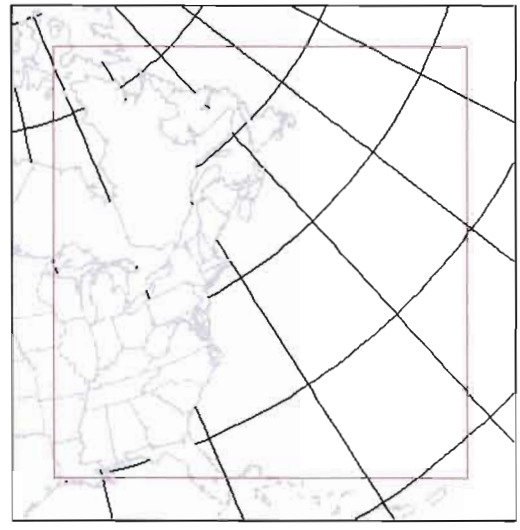

Fig. 1 The integration domain of the CRCM. The ribbon outside the red line denotes the relaxation zone that is excluded from the analysis.

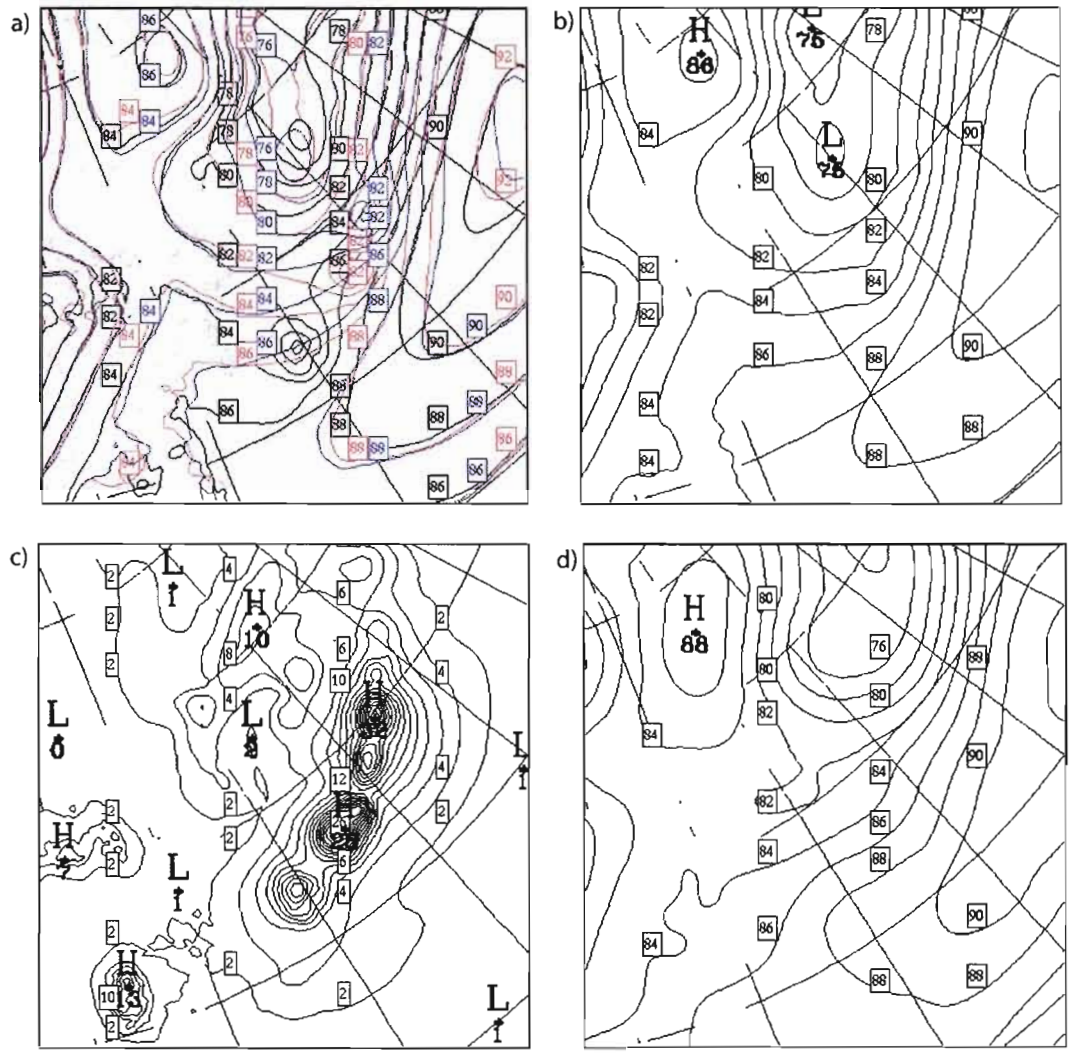

Fig. 2 Geopotential height at 925 hPa on 1993.07.25 at 0000UTC: *(a)* three selected realizations (in *dam*); *(b)* the ensemble mean of the 20 realizations (in *dam*); *(c)* the standard deviation of the ensemble (in *m*); *(d)* NCEP reanalyses projected on the CRCM grid (in *dam*).

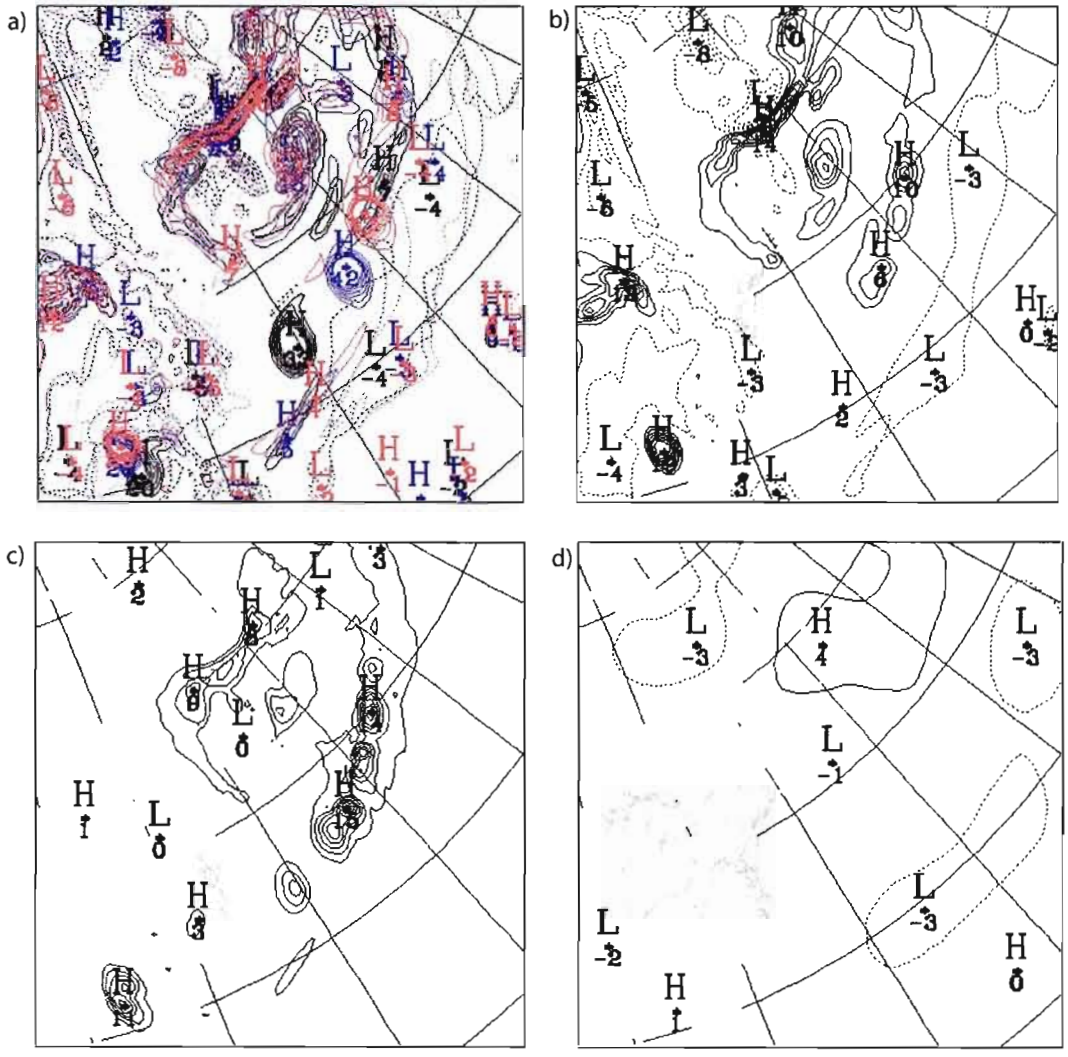

Fig. 3 Relative vorticity at 925 hPa on 1993.07.25 at 0000UTC (in 10^{-5} s^{-1}): *(a)* three selected realizations; *(b)* the ensemble average of the 20 realizations; *(c)* the standard deviation of the ensemble; *(d)* regridded NCEP reanalyses. Full lines for positive values and dotted for negative of relative vorticity.

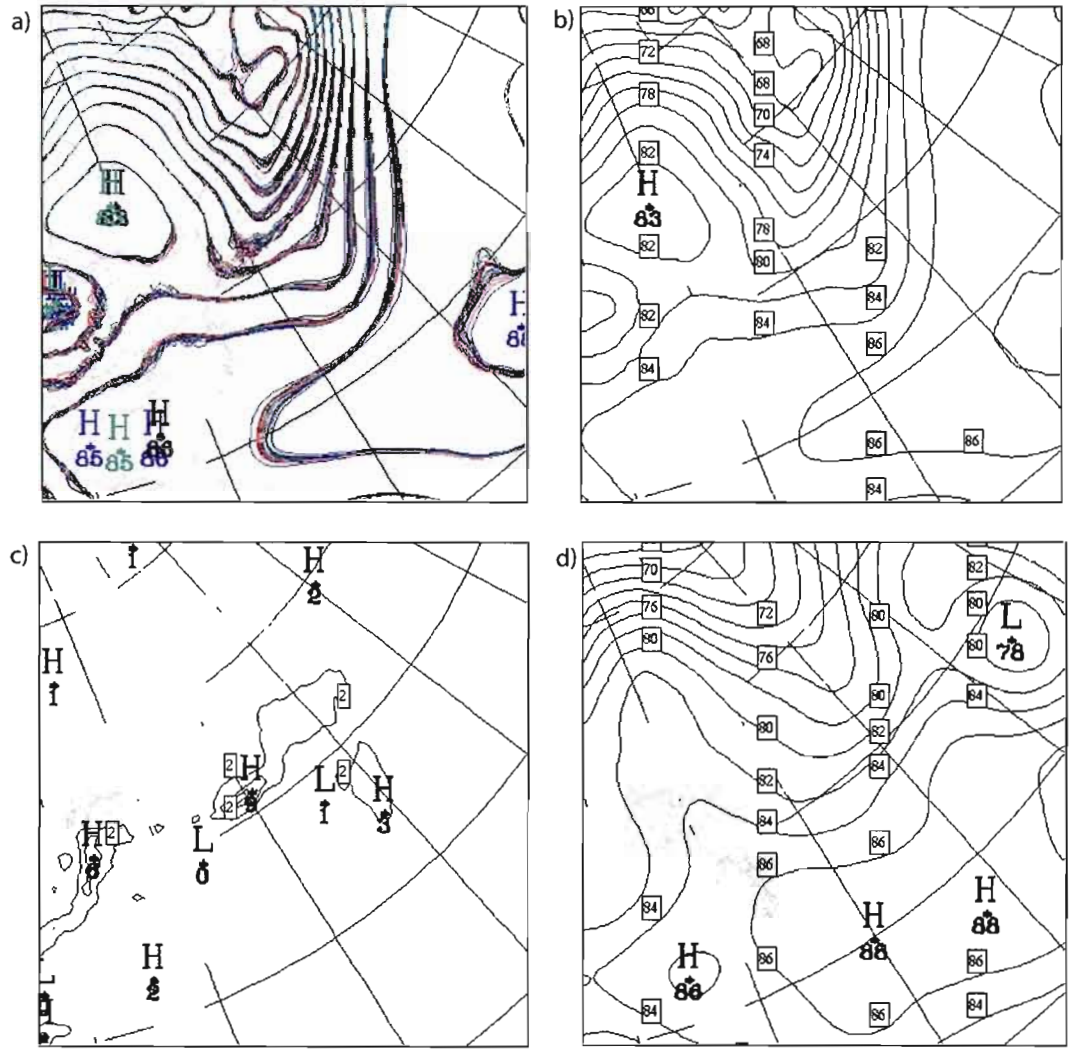

Fig. 4. Geopotential height at 925 hPa on 1993.06.20 at 0000UTC: *(a)* 20 individual realizations (in *dam*); *(b)* the ensemble average (in *dam*); *(c)* the standard deviation of the ensemble (in *m*); *(d)* regridded NCEP reanalyses (in *dam*).

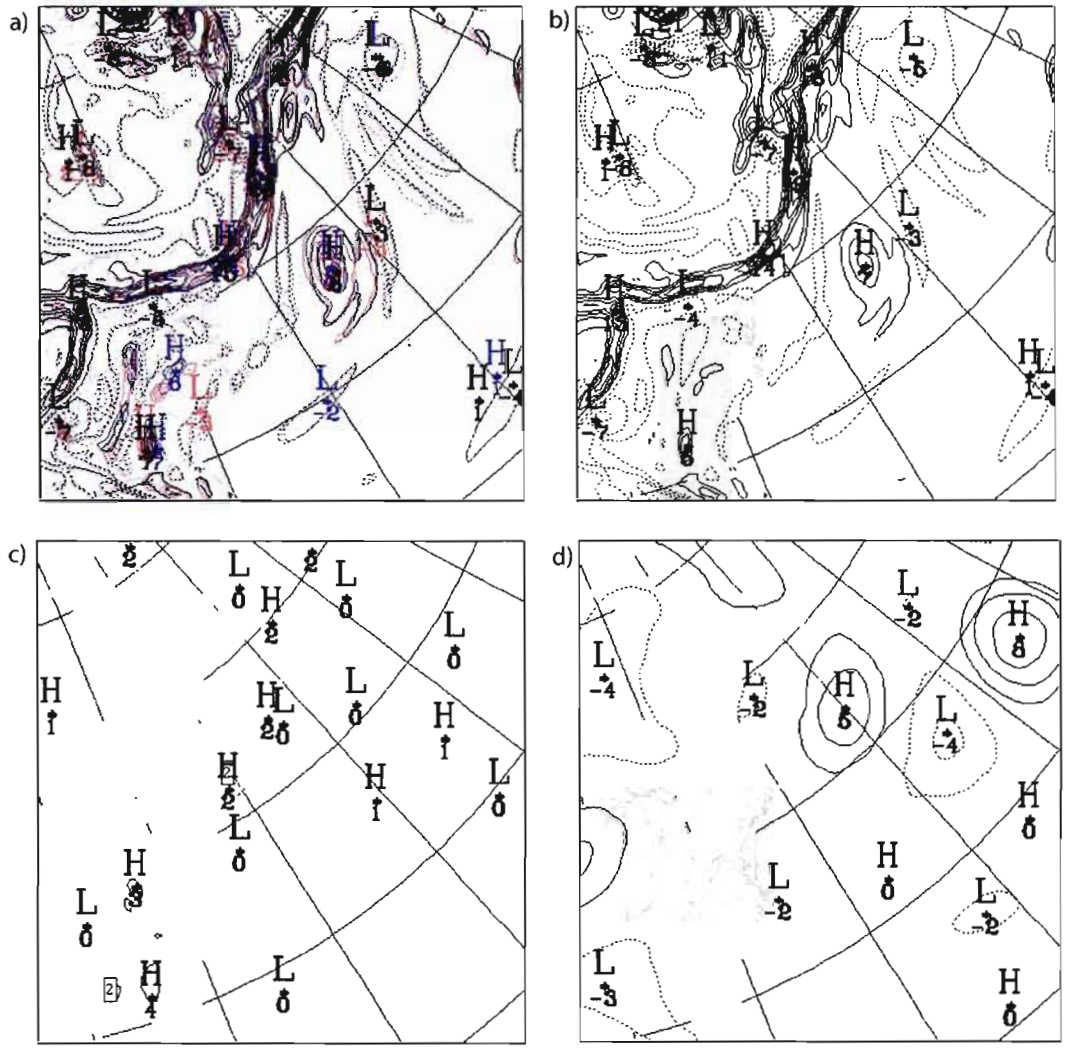

Fig. 5 Relative vorticity at 925 hPa on 1993.06.20 at 0000UTC (in 10^{-5} s^{-1}): *(a)* three selected realizations; *(b)* the ensemble average of the 20 realizations; *(c)* the standard deviation of the ensemble; *(d)* regridded NCEP reanalyses. Full lines for positive values and dotted for negative values of relative vorticity.

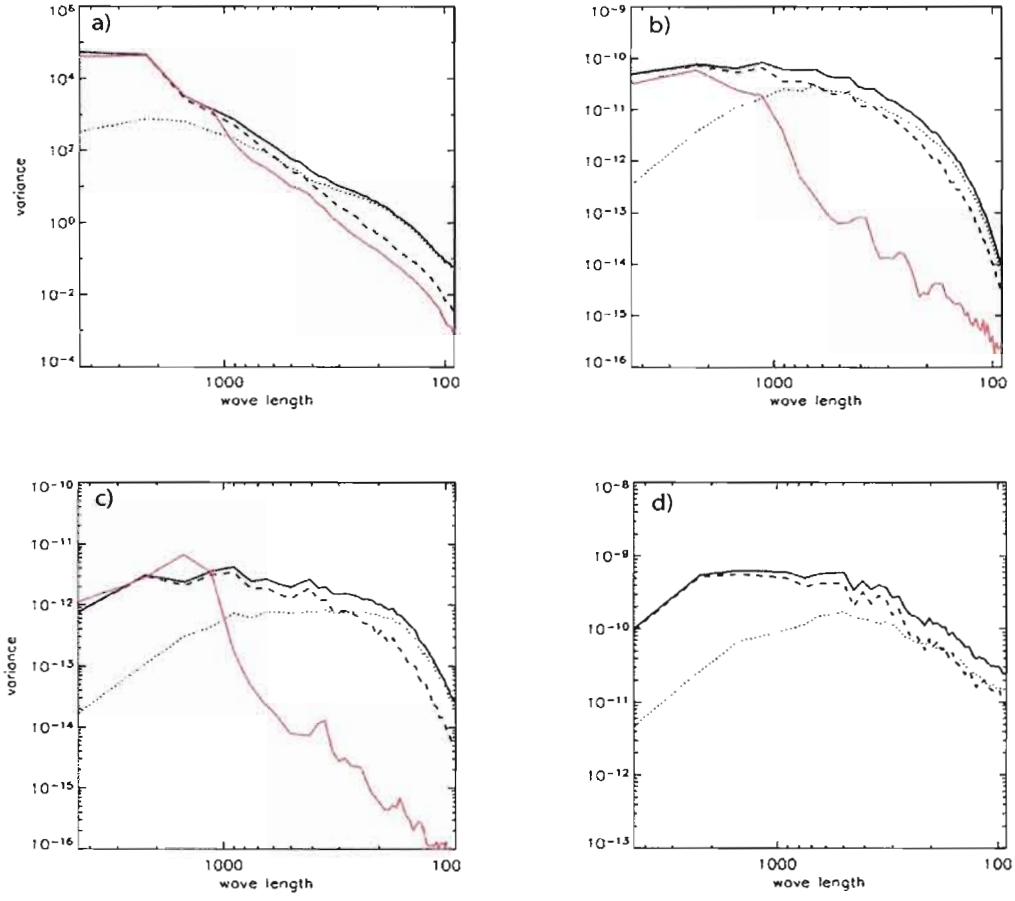

Fig. 6 Decomposition of power spectra at 925 hPa on *1993.07.25* at *0000UTC* of: *(a)* geopotential height, *(b)* vorticity, *(c)* divergence, and *(d)* precipitation. *Full* line represents the ensemble average of members power spectra defined in Equation (5), *dashed* – its reproducible part (6), and *dotted* – its irreproducible part (7). The *red* line is the spectral variance of the regridded NCEP reanalyses (not available for precipitation).

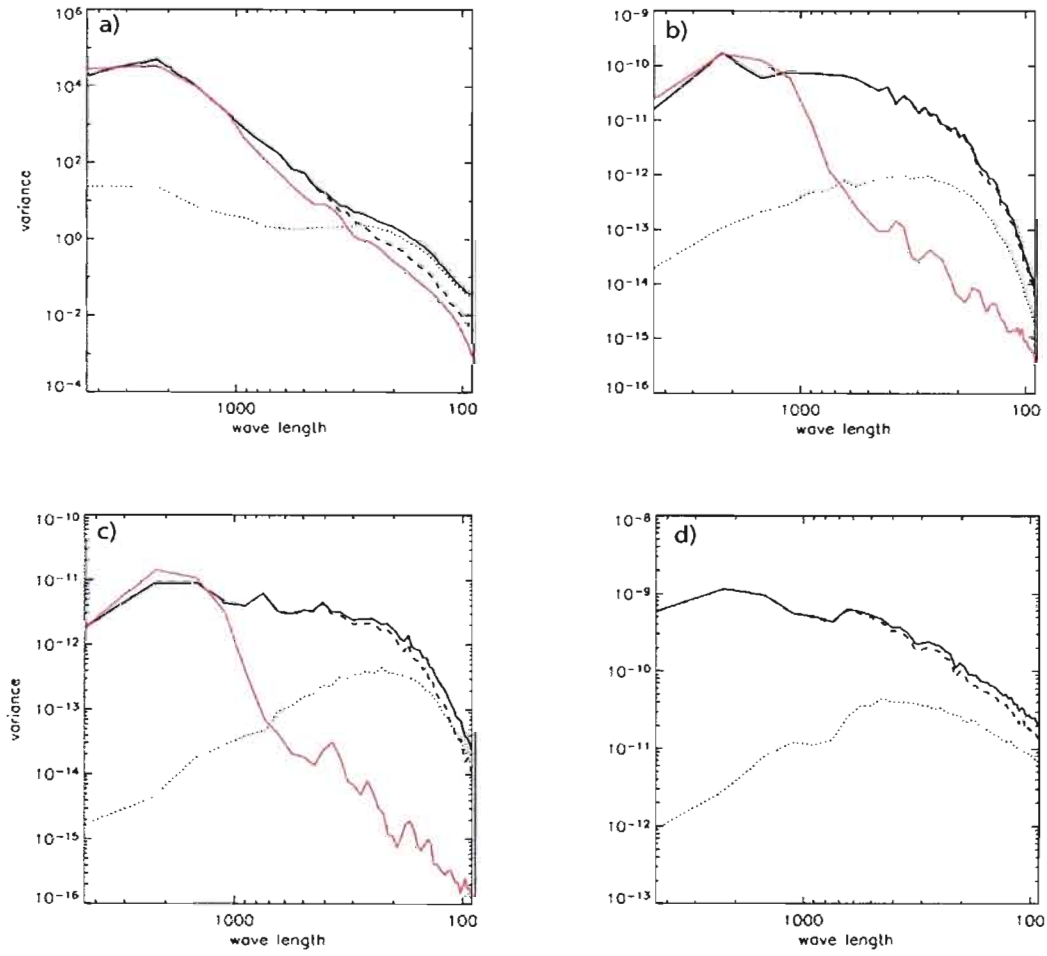

Fig. 7 Decomposition of power spectra at 925 hPa on 1993.06.20 at 0000UTC of: *(a)* geopotential height, *(b)* vorticity, *(c)* divergence, and *(d)* precipitation. *Full* line represents the ensemble average of members power spectra defined in Equation (5), *dashed* – its reproducible part (6), and *dotted* – its irreproducible part (7). The *red* line is the spectral variance of the regridded NCEP reanalyses (not available for precipitation).

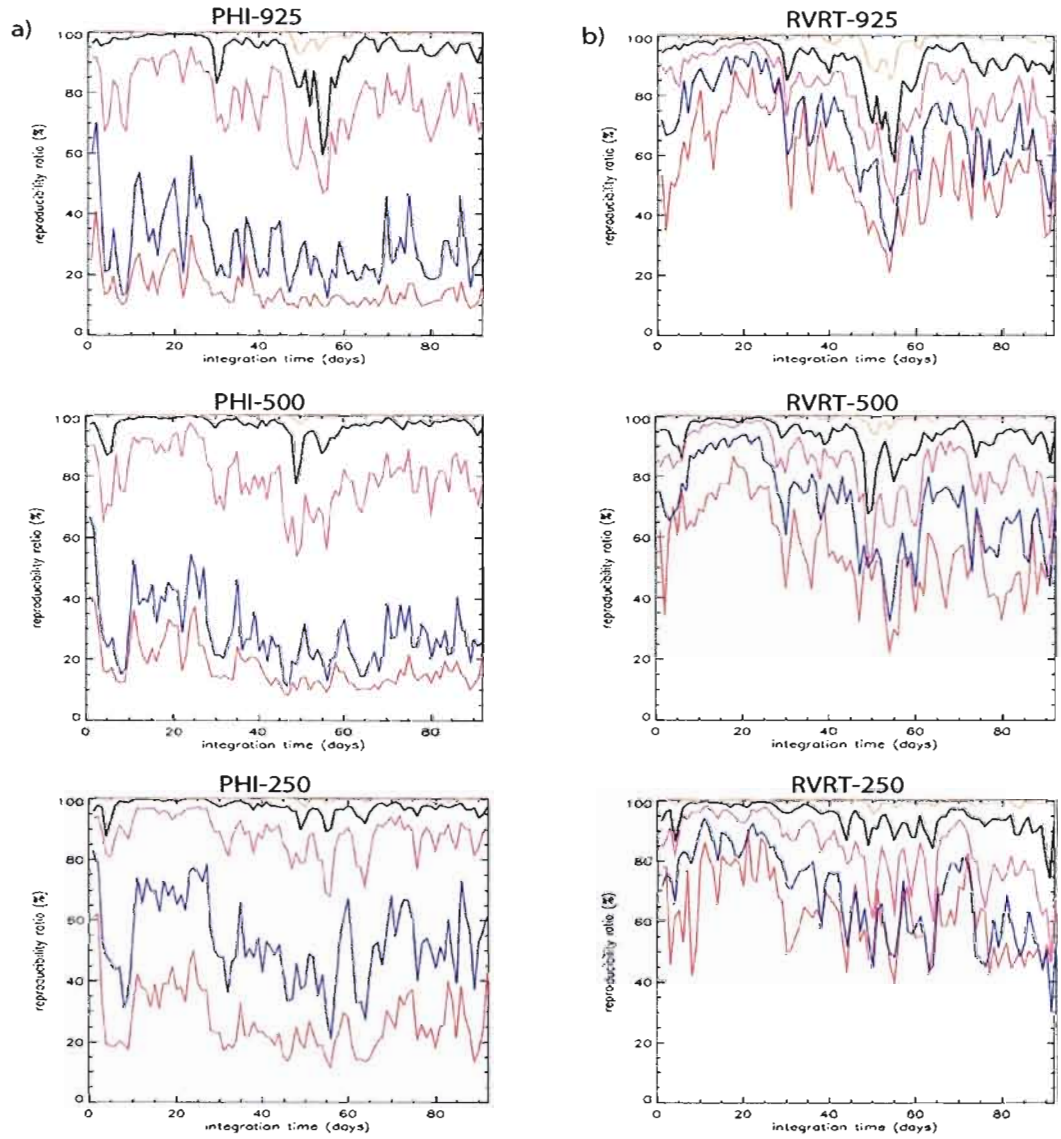

Fig. 8 Reproducibility ratio as a function of time at different length scales for: *(a)* geopotential height, *(b)* vorticity *(c)* divergence, and *(d)* precipitation, at levels of 925, 500 and 250 hPa, and *(b)* precipitation; *yellow*: 2250 km (wavenumber 2); *black*: 900 km (wavenumber 5); *purple*: 450 km (wavenumber 10); *blue*: 225 km (wavenumber 20); *red*: 100 km (wavenumber 45).

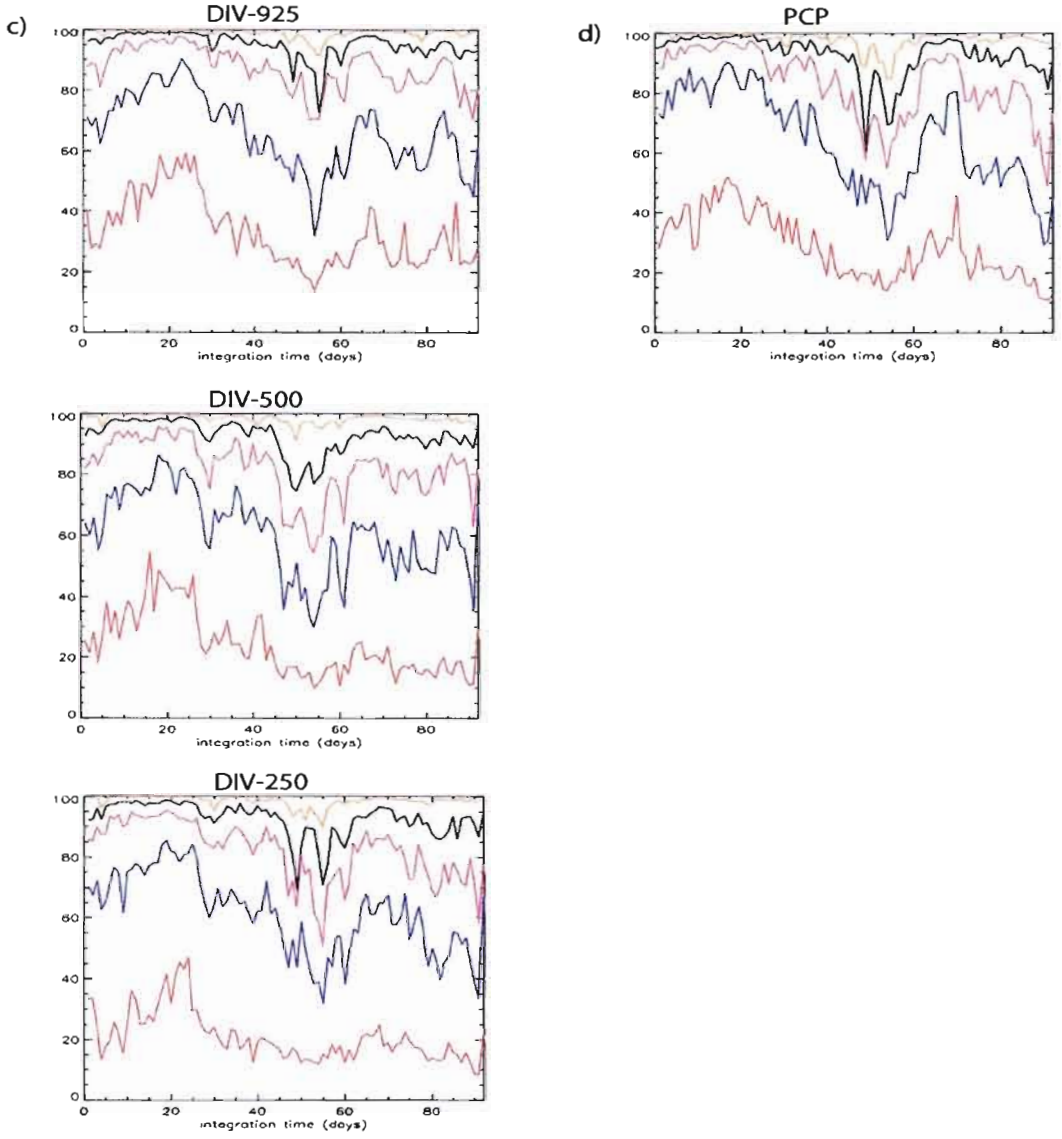

Fig. 8 (Continued)

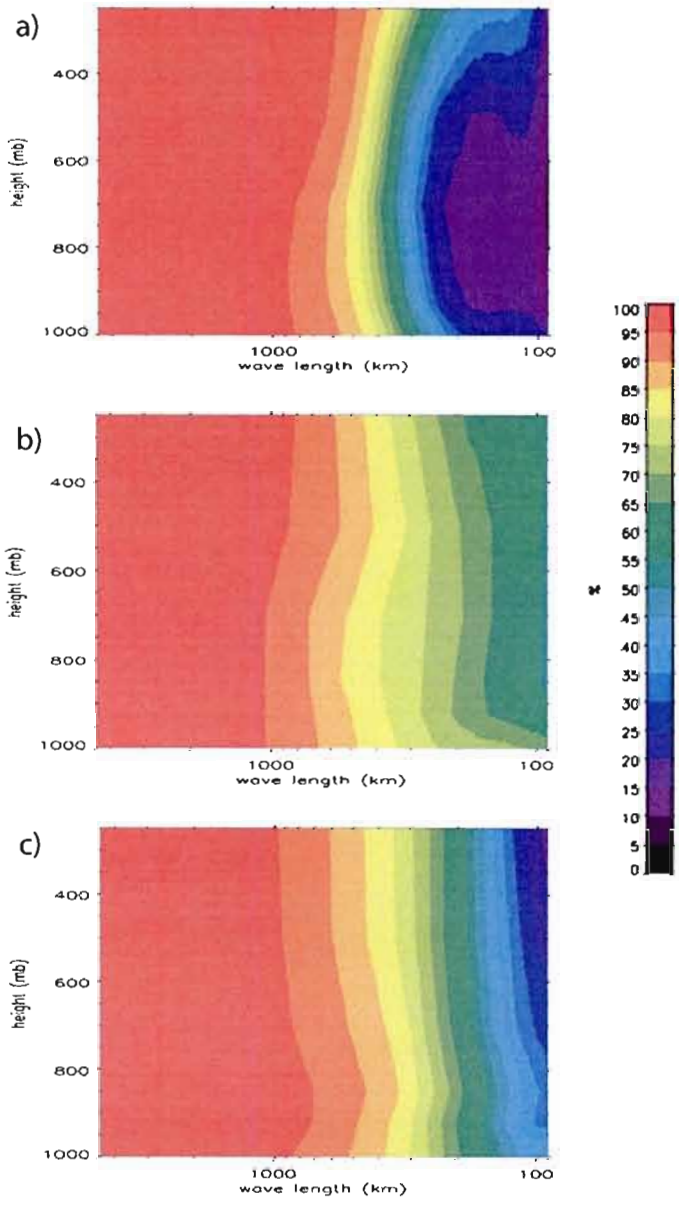

Fig. 9 Representative time-average reproducibility ratio (in %) as a function of length scale and height, for: *(a)* geopotential height, *(b)* relative vorticity and *(c)* divergence.

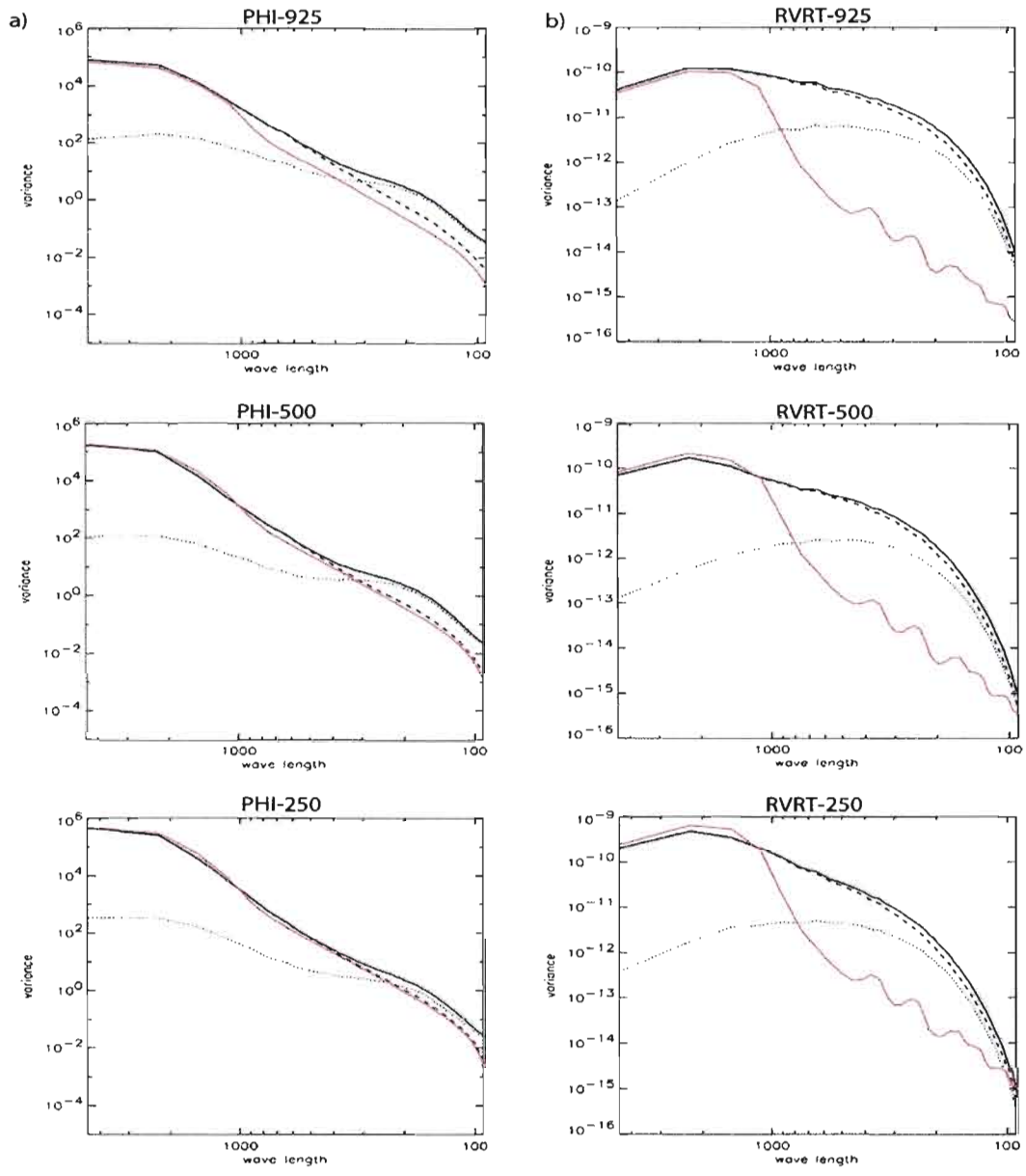

Fig. 10 Time-average power spectra of *(a)* geopotential height, *(b)* vorticity, *(c)* divergence at 925, 500 and 250 hPa, and *(d)* precipitation. *Full* line $\overline{S^A}$, *dashed* line $\overline{S^R}$, *dotted* line $\overline{S^I}$ and *red* line NCEP reanalyses projected on the CRCM grid.

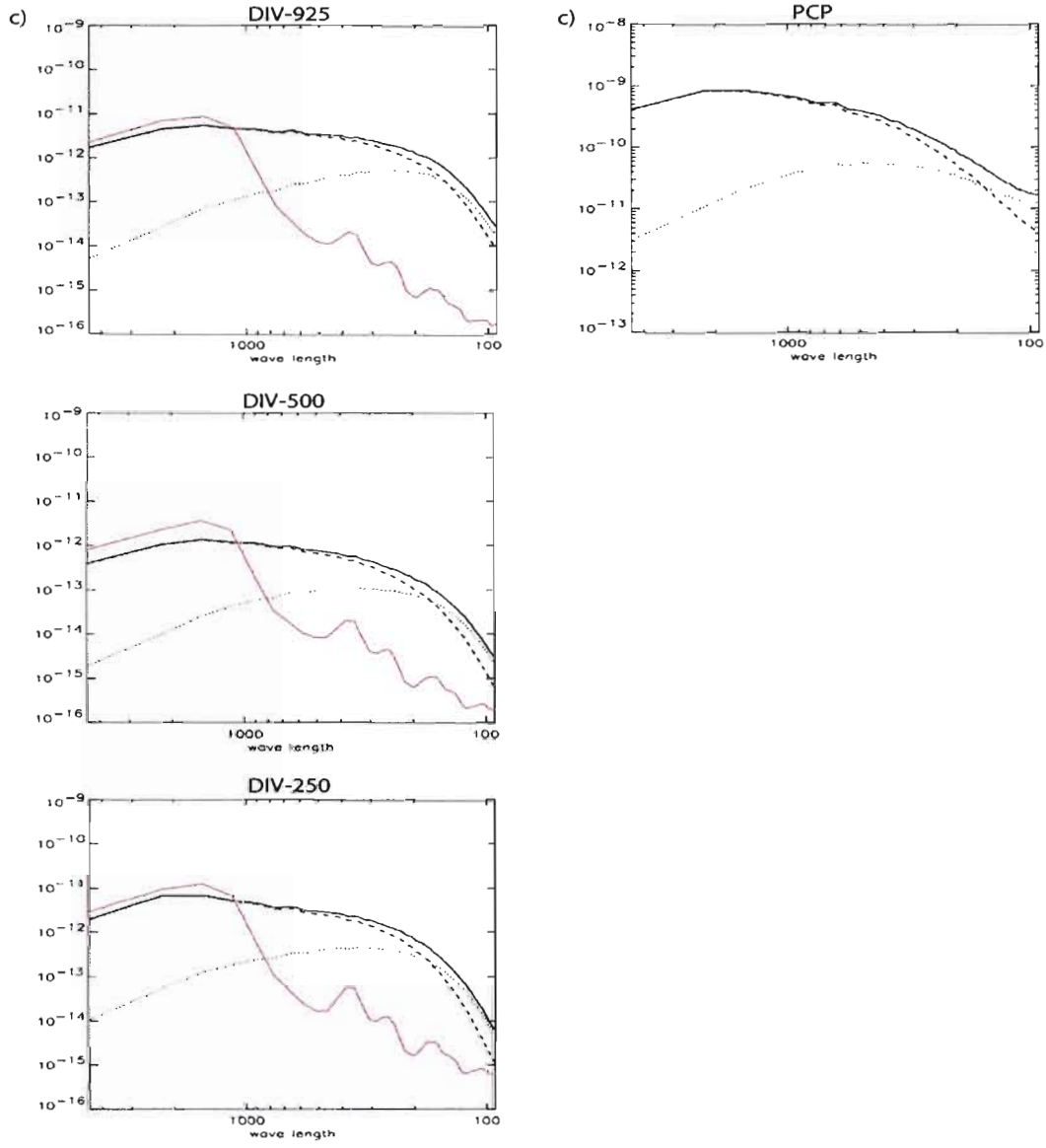

Fig. 10 (Continued)

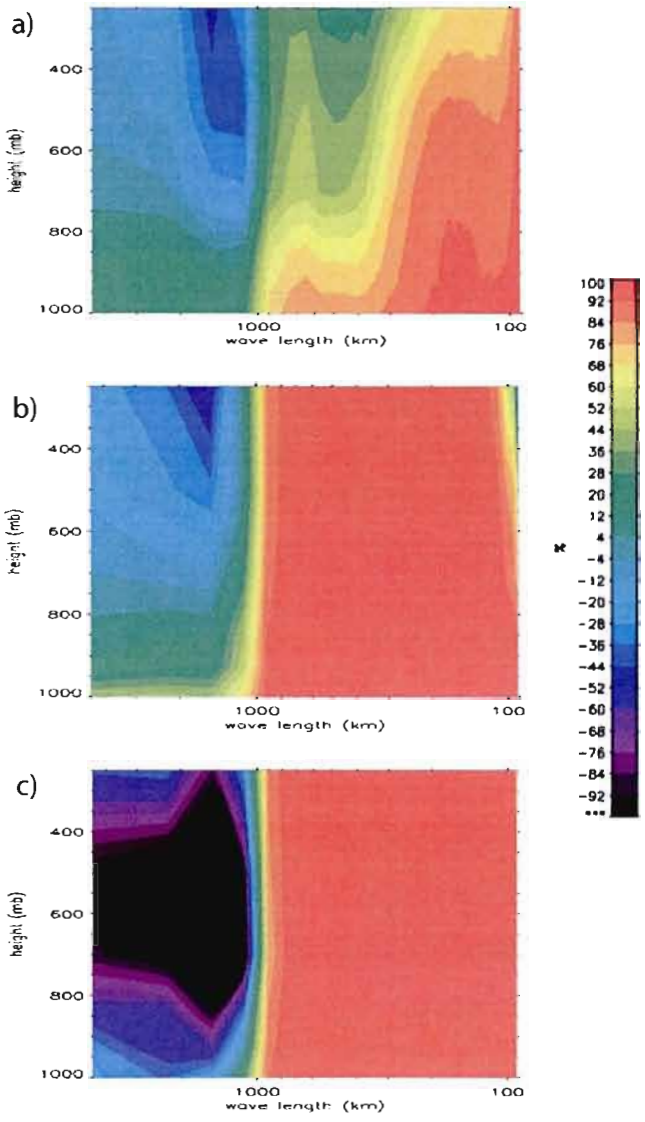

Fig. 11 Accrued amplitude of CRCM fields with respect to the NCEP reanalyses, η (defined in Equation 12, in %), as a function of length scale and height, for: *(a)* geopotential height, *(b)* relative vorticity *(c)* divergence.

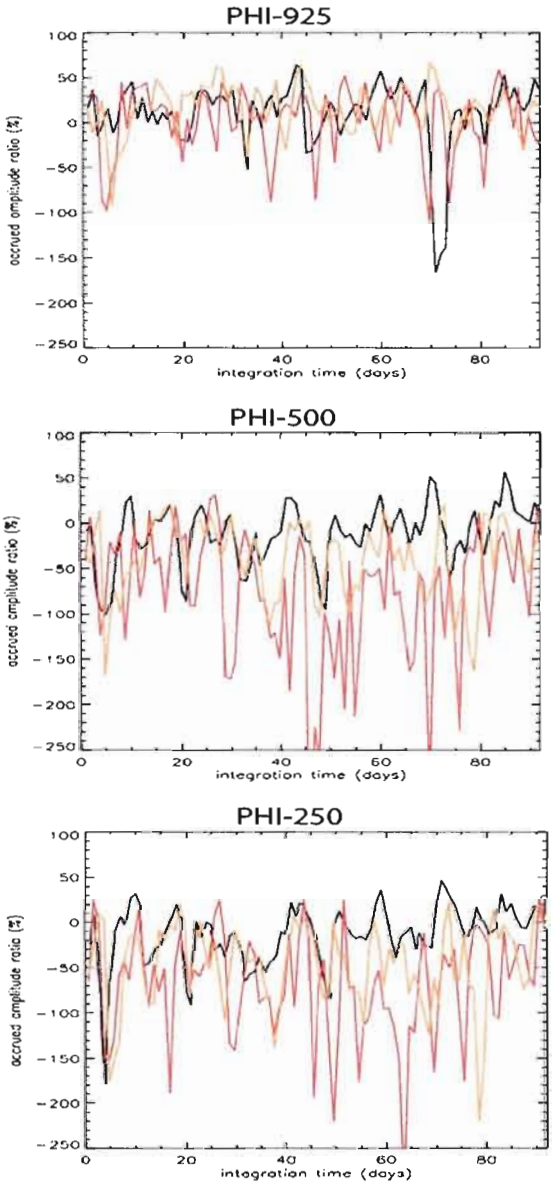

Fig. 12 Instantaneous accrued amplitude η_k as a function of time at different length scales for: geopotential height at 925, 500 and 250 hPa; *black*: 4500 km (wavenumber 1); *yellow*: 2250 km (wavenumber 2); and *red*: 1125 km (wavenumber 4).

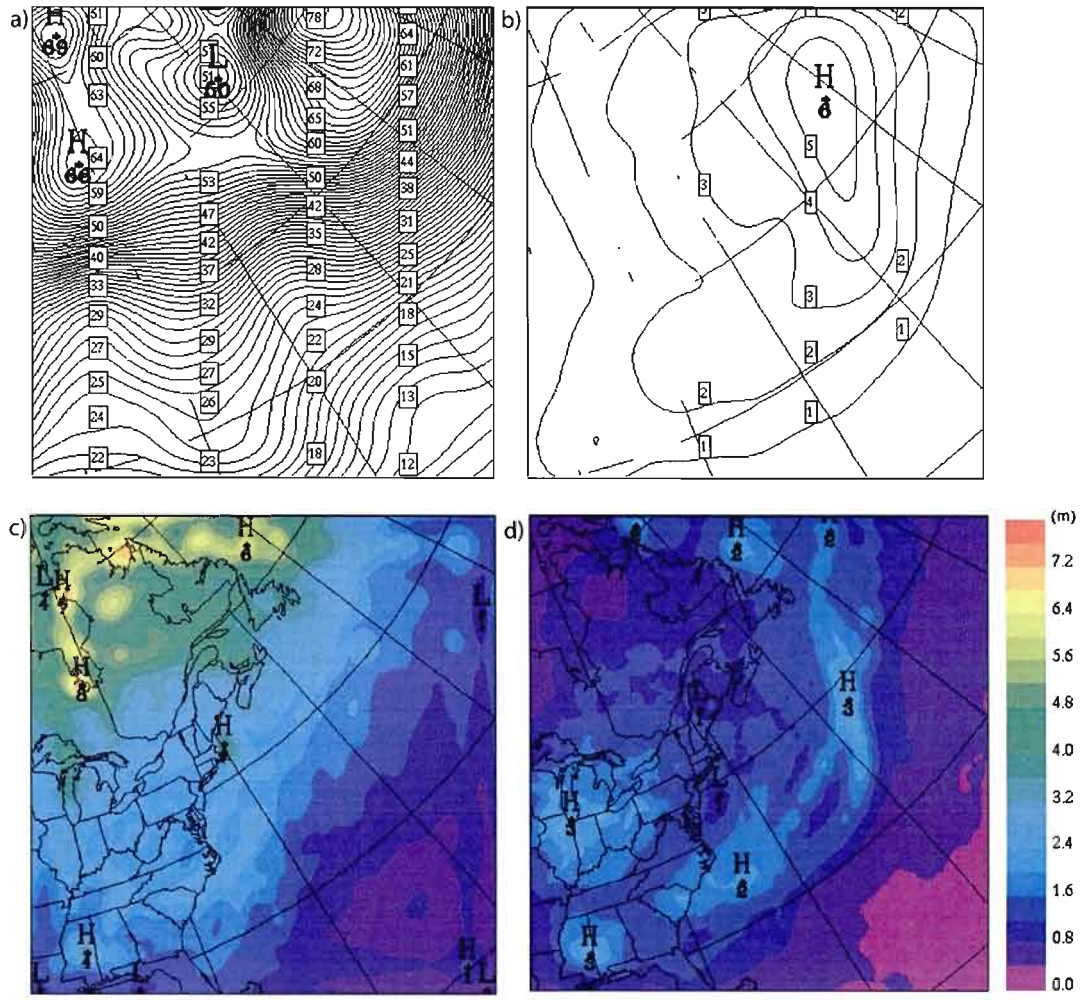

Fig. 13 Transient eddy standard deviation of geopotential height at 925 hPa (in *m*): *(a)* reproducible large-scale component, *(b)* irreproducible large-scale component, *(c)* reproducible small-scale component and *(d)* irreproducible small-scale component.

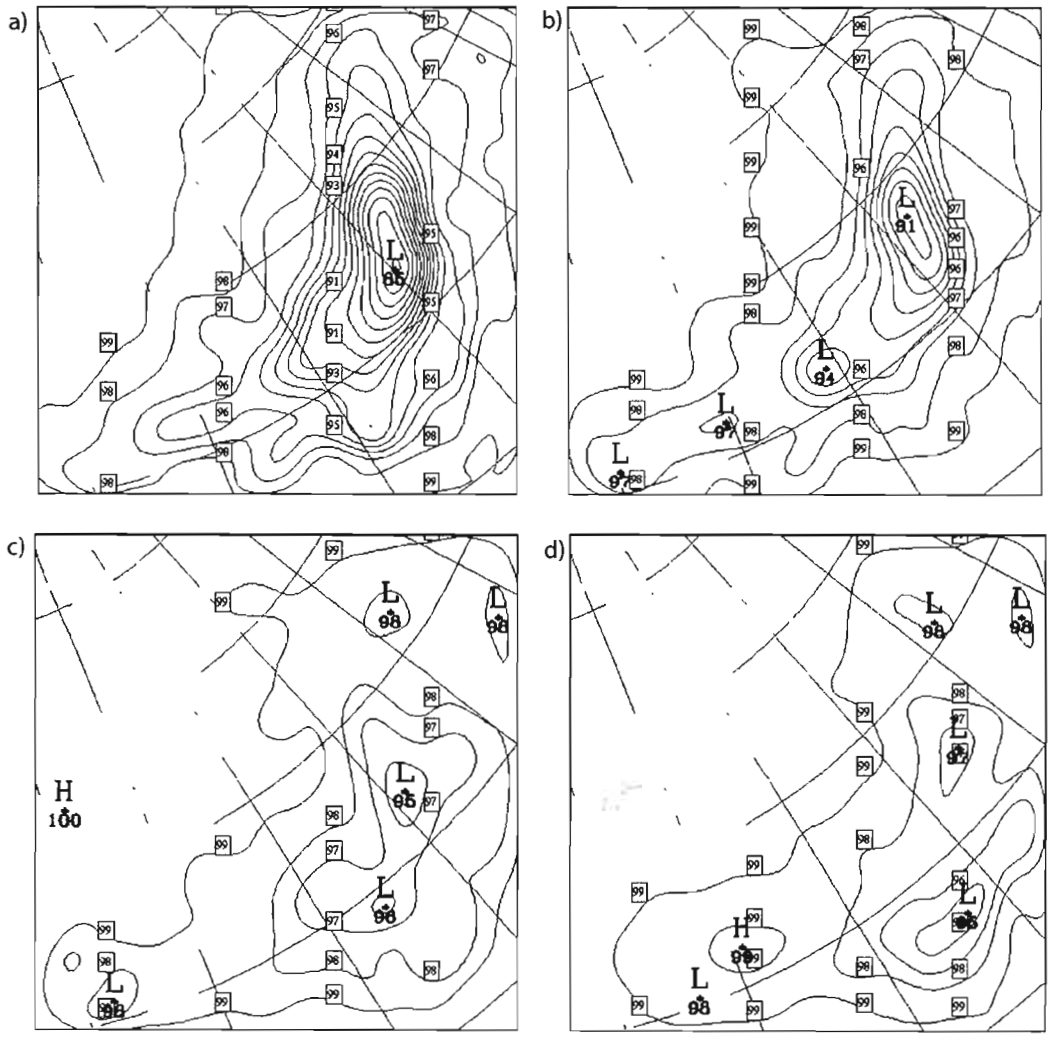

Fig. 14 Reproducibility ratio of transient-eddy variance of large-scale components of relative vorticity (in %): *(a)* 925 hPa, *(b)* 700 hPa, *(c)* 500 hPa and *(d)* 250 hPa.

Fig. 15 Reproducibility ratio of transient-eddy variance of large-scale divergence (in %) at: *(a)* 925 hPa, *(b)* 700 hPa, *(c)* 500 hPa and *(d)* 250 hPa.

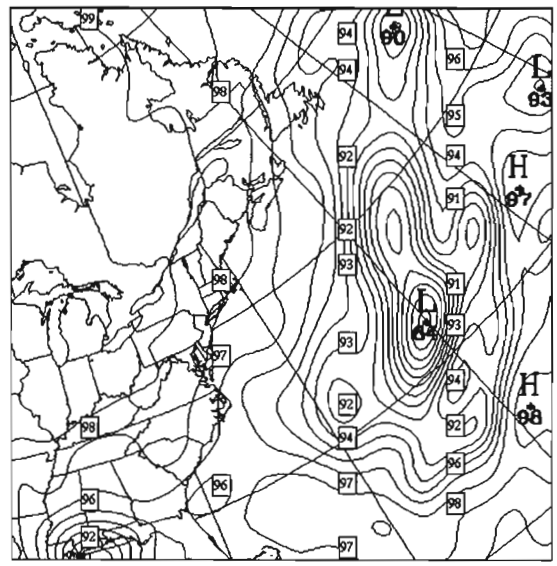

Fig. 16 Reproducibility ratio of transient-eddy variance of large-scale precipitation (in %).

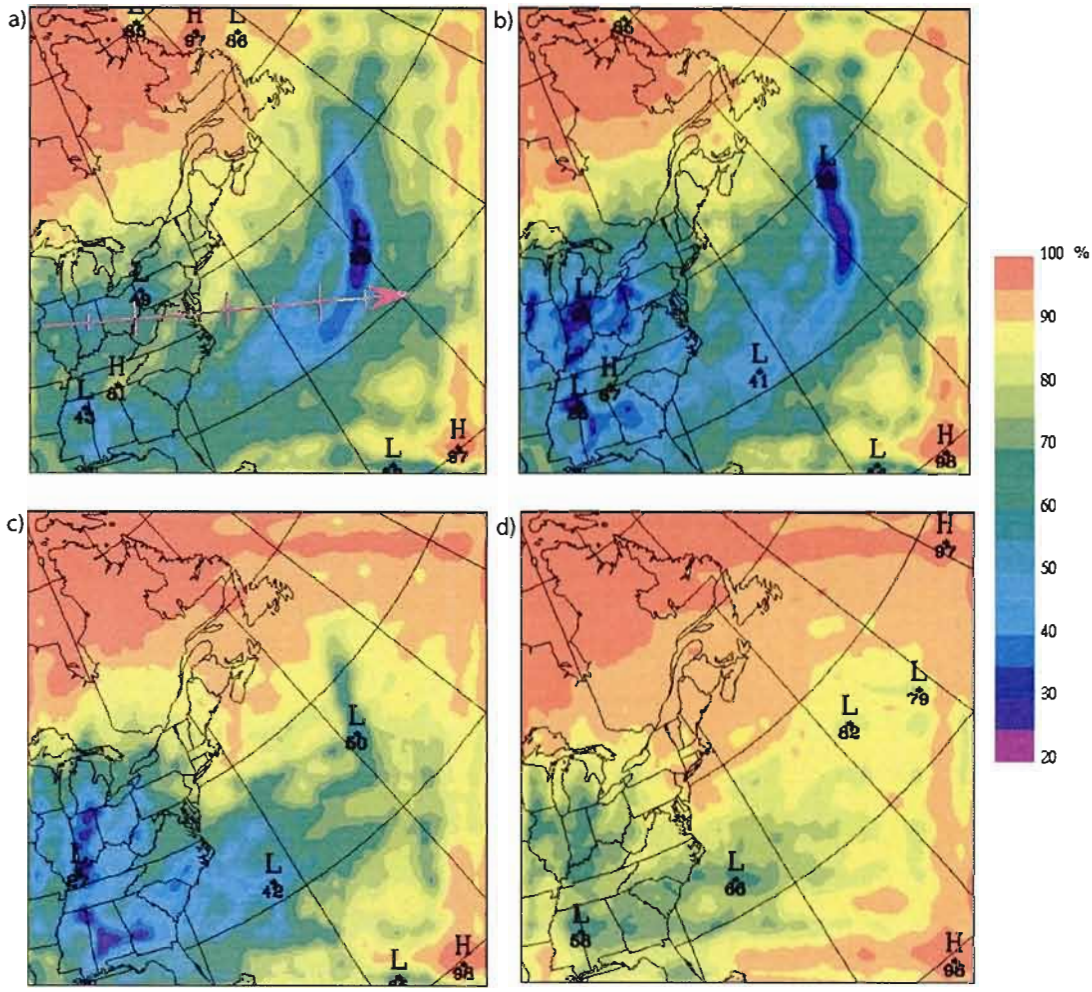

Fig. 17 Reproducibility ratio of transient-eddy variance of small-scale components of geopotential height (in %): *(a)* 925 hPa, *(b)* 700 hPa, *(c)* 500 hPa and *(d)* 250 hPa. The vertical cross-section along the arrow shown in (a) is presented in (e).

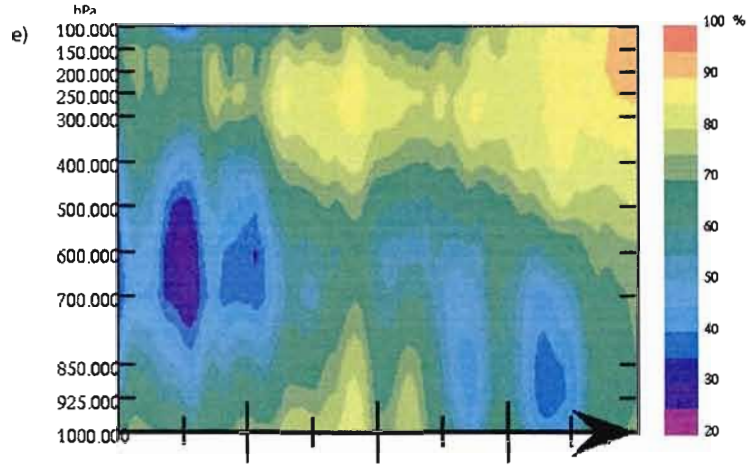

Fig. 17 (Continued)

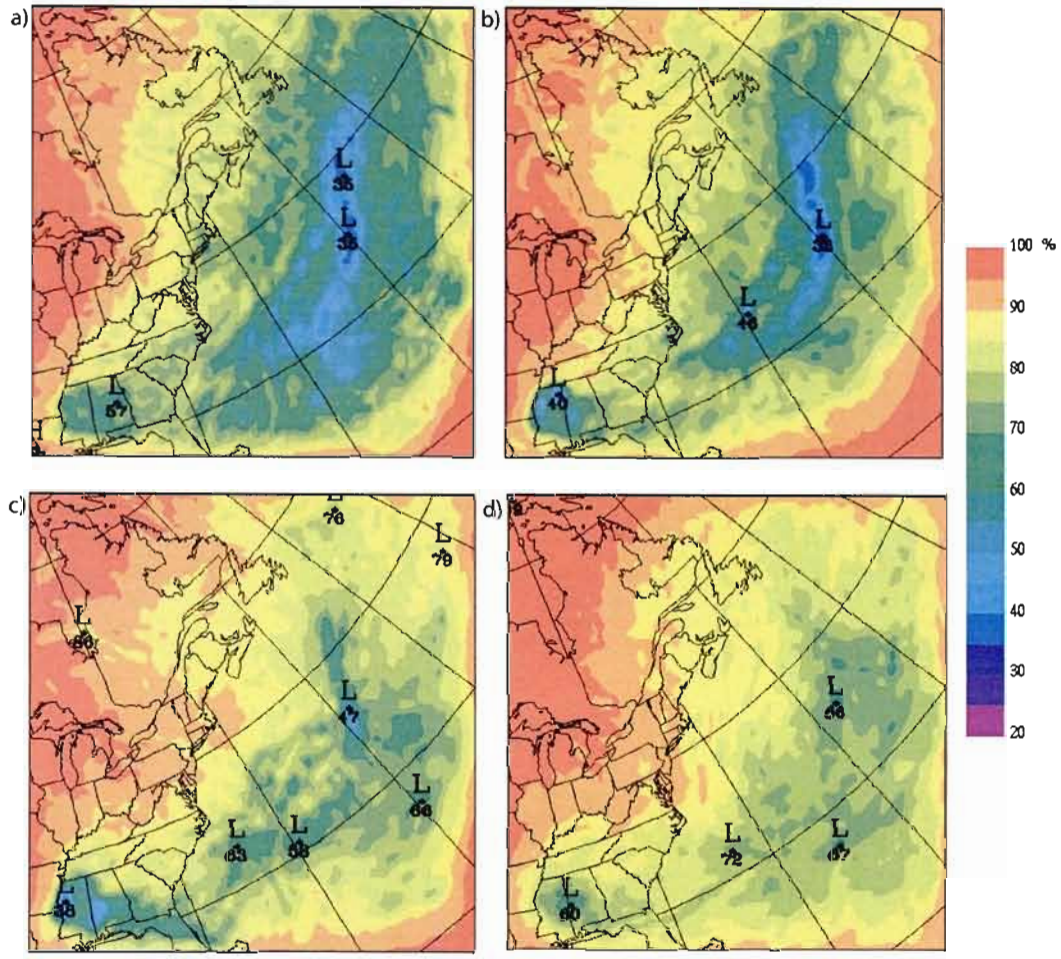

Fig. 18 Reproducibility ratio of transient-eddy variance of small-scale relative vorticity (in %) at: *(a)* 925 hPa, *(b)* 700 hPa, *(c)* 500 hPa and *(d)* 250 hPa.

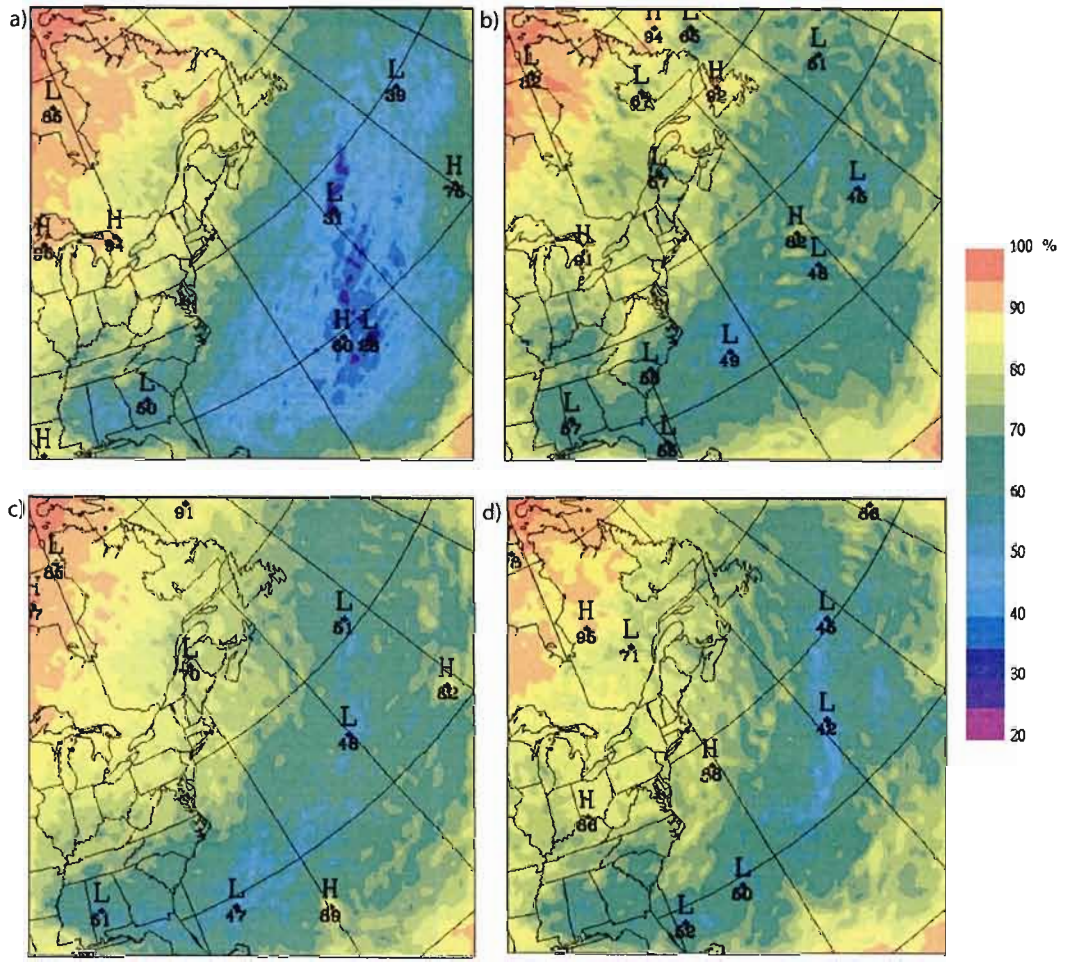

Fig. 19 Reproducibility ratio of transient-eddy variance of small-scale divergence (in %) at: *(a)* 925 hPa, *(b)* 700 hPa, *(c)* 500 hPa and *(d)* 250 hPa.

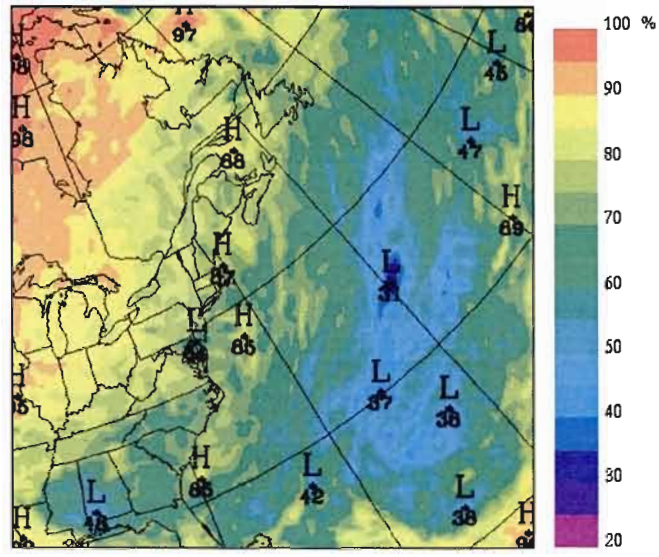

Fig. 20 Reproducibility ratio of transient-eddy variability of small-scale precipitation (in %).

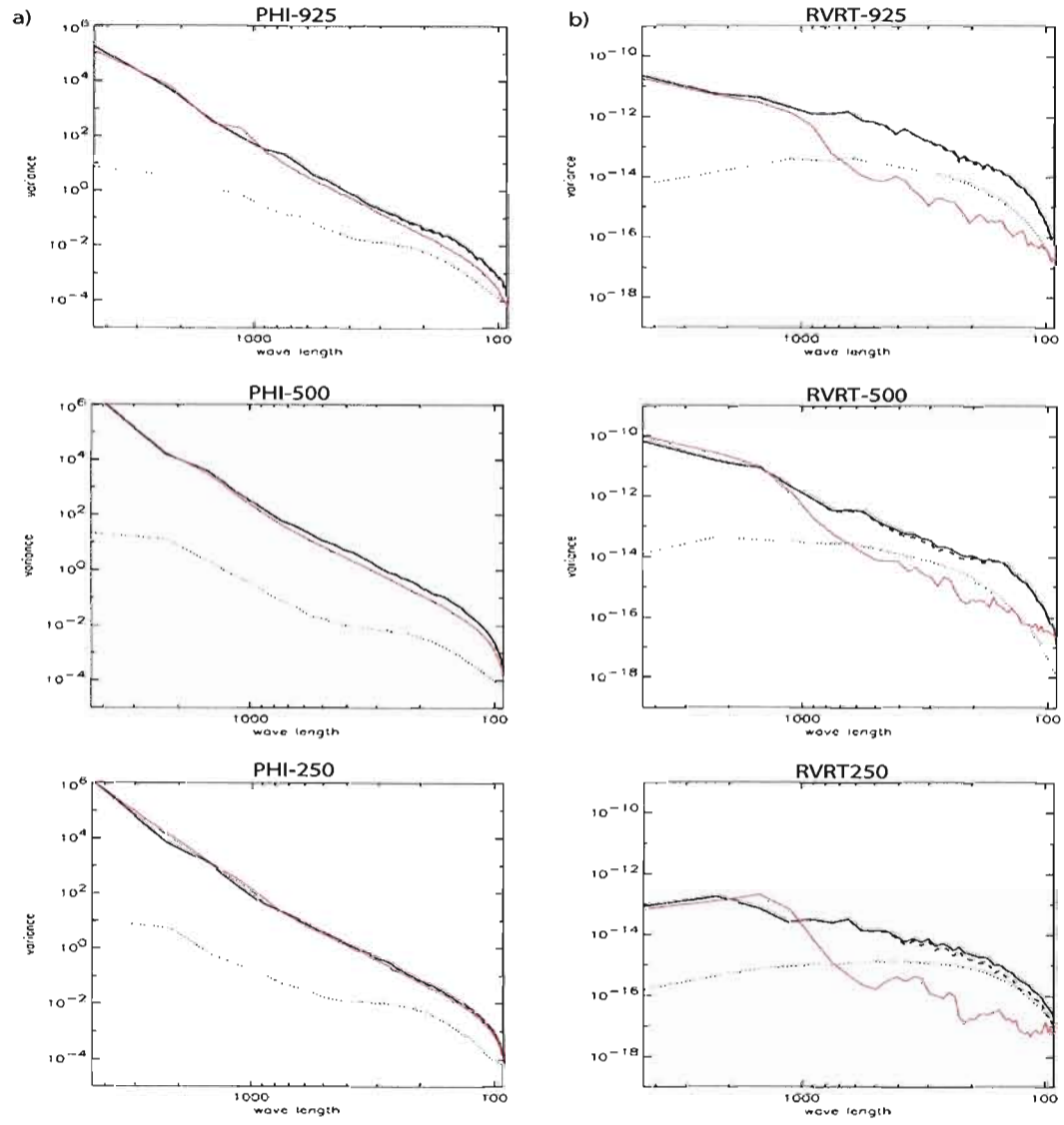

Fig. 21 Time average power spectra of: *(a)* geopotential height, *(b)* relative vorticity, *(c)* divergence at 925, 500, and 250 hPa, and *(d)* precipitation. *Full* line represents the ensemble--average power spectrum defined in Equation (5), *dashed* – its reproducible part (6), and *dotted* – its irreproducible part (7). The *red* line is the power spectrum of NCEP reanalyses (not available for precipitation).

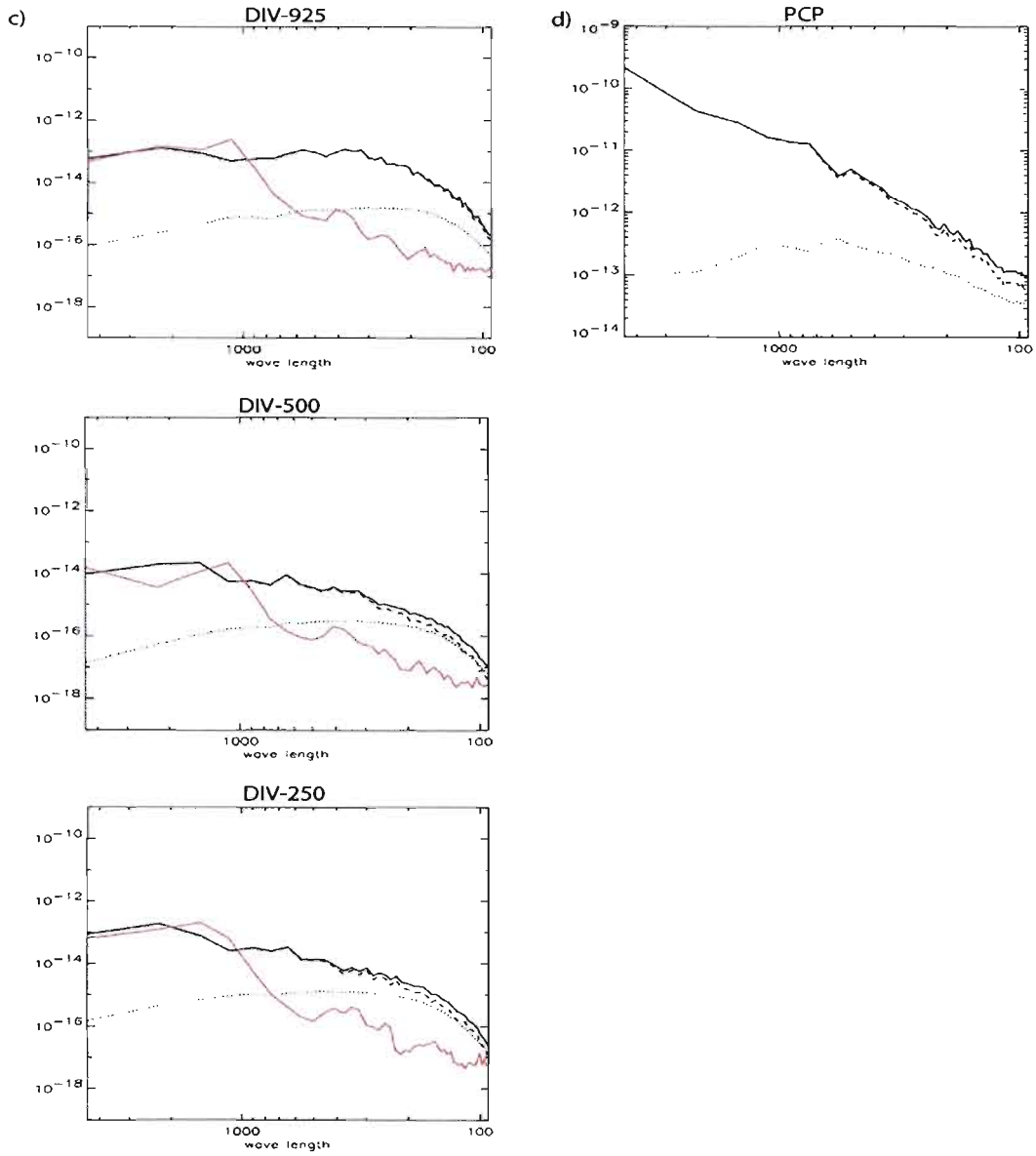

Fig. 21 (Continued)

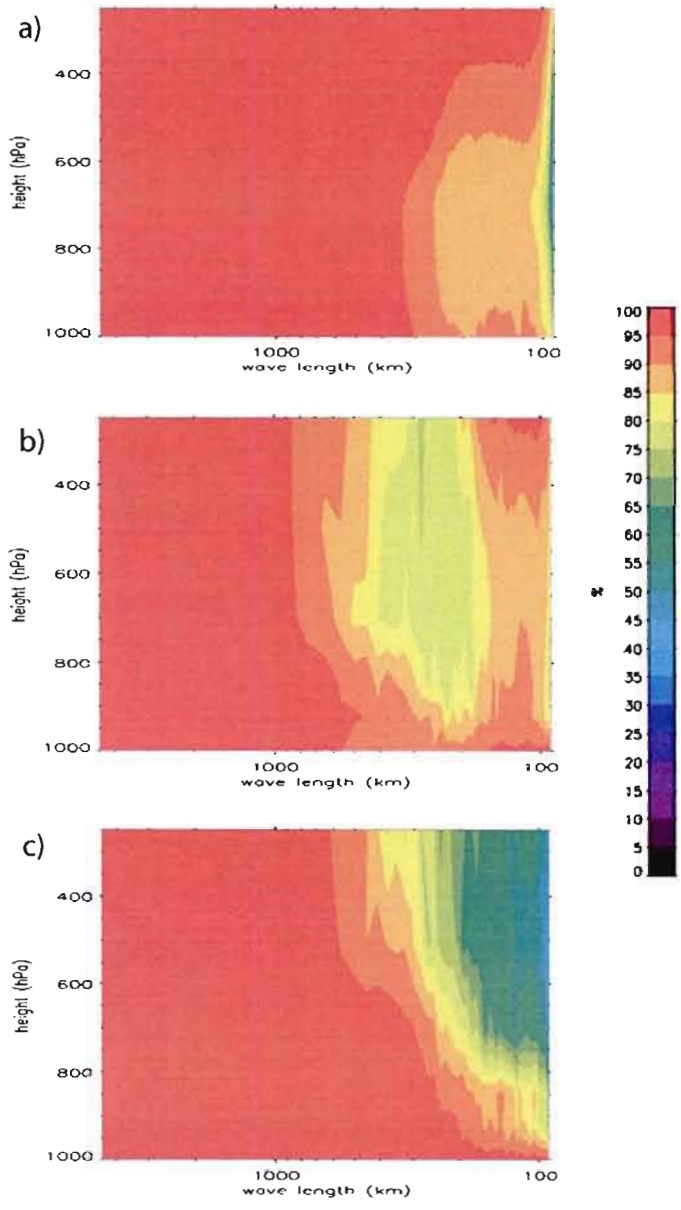

Fig. 22 Reproducibility ratio of seasonal average (in %) as function of length scale and height, for: *(a)* geopotential height, *(b)* relative vorticity, and *(c)* divergence.

CONCLUSION

Le but de ce travail est d'identifier les composantes reproductibles et non-reproductibles des champs générés par un MRC. La composante reproductible est définie comme celle qui est générée de façon déterministe, indépendant des perturbations dans les conditions initiales. Elle est associée au forçage par les conditions de frontières. Par contre, la composante non-reproductible est affectée par la variabilité interne, et est considérée comme libre, dans un sens déterministe, des conditions de frontières.

Dans la présente étude, un ensemble de 20 intégrations du Modèle Régional Canadien de Climat (MRCC), pilotées par les analyses de NCEP, est effectué pour une saison d'été au-dessus d'un domaine centré aux latitudes moyennes. Les variables du modèle et leurs moyennes saisonnières sont ensuite décomposées en composantes reproductibles et non-reproductibles. La première est identifiée par la moyenne d'ensemble tandis que la deuxième est obtenue à partir des déviations des membres de l'ensemble par rapport à la moyenne d'ensemble. L'étude examine comment le MRCC partage sa variabilité spatio-temporelle entre les deux composantes.

Les résultats montrent que la variabilité interne dépend fortement de l'échelle spatiale des perturbations. Les plus petites échelles sont les plus affectées. Par contre, l'écoulement est considérablement contraint par des CFL aux grandes échelles de plus de 1000 km. La composante reproductible y apporte beaucoup plus informations que la composante non-reproductible. Par intermittence, la variabilité interne pénètre la région spectrale des grandes échelles en augmentant significativement l'intensité relative de la composante non-reproductible.

En plus, la reproductibilité élevée de grandes échelles est présente dans toutes les variables et elle est minimale aux bas niveaux. Ce phénomène pourrait être dû à une augmentation du temps de résidence de l'air à l'intérieur du domaine à cette altitude, à cause de vents plus faibles. Par contre, la reproductibilité de petites échelles de l'ordre de *100km* est légèrement plus grande aux bas niveaux. Ceci peut être associé au forçage de fine échelle exercé par la frontière inférieure. Néanmoins, l'absence d'une grande reproductibilité des petites échelles des variables de surface implique que, dans l'ensemble étudié, le forçage par la surface ne contraint pas considérablement la variabilité interne du modèle.

Les perturbations transitoires de grande échelle montrent, pour toutes les variables, le même patron spatial de la reproductibilité: la reproductibilité est en général grande à proximité des frontières d'entrée et elle diminue en aval. La distribution spatiale de reproductibilité des petites échelles suit principalement celle des grandes échelles, mais les valeurs sont considérablement plus petites. De même, la variation temporelle de la reproductibilité des petites échelles est relativement bien synchronisée avec celle de la reproductibilité de grandes échelles. C'est particulièrement le cas pour le tourbillon relatif pour lequel les reproductibilités de grandes et petites échelles semblent être étroitement liées. La reproductibilité des petites échelles du géopotentiel a des minimums additionnels situés au-dessus de la surface continentale chaude, dans les régions où la reproductibilité des grandes échelles est très forte. Cette région pourrait représenter une source de variabilité interne des petites échelles où la convection génère des petites perturbations qui sont différentes dans chacune des réalisations de l'ensemble.

De plus, la comparaison des spectres de puissance du MRCC et les analyses NCEP est effectuée pour les variables instantanées. Cela indique que la variabilité spatiale du MRCC aux grandes échelles (qui sont représentées par les données de pilotage) est en moyenne légèrement surestimée près de la surface. Par contre, elle pourrait être considérablement sous-estimée dans la troposphère supérieure. Ceci justifierait le besoin d'appliquer le pilotage des grandes échelles à l'intérieur du domaine du MRCC. Cependant, il reste à examiner si le pilotage interne de grandes échelles supprimerait la génération des petites échelles et comment elle influence leur variabilité interne.

L'analyse des moyennes saisonnières (perturbations stationnaires) prouve que la composante reproductible domine le spectre entier. Près de la surface, les échelles plus grandes que *200km* de toutes les variables du MRCC sont générées sous forme reproductible. Cependant, aux niveaux supérieurs et aux échelles plus petites que 200km, la composante non-reproductible devient non négligeable. Cela se reflète dans une reproductibilité relativement basse de la précipitation saisonnière à ces échelles.

RÉFÉRENCES

Alexandru A., R. de Elía and R. Laprise, 2007: Internal variability in Regional Climate Downscaling at the seasonal scale. *Mon. Wea. Rev.*, **135**, 3221–3238.

Anthes, R. A., Y. H. Kuo, D. P. Baumhefner, R. M. Errico and T. W. Bettge, 1985: Predictability of Mesoscale Atmospheric Motions. *Advances Geophys.*, **288**, Academic Press, 159-202.

Biner, S., D. Caya, R. Laprise and L. Spacek, 2000: Nesting of RCMs by imposing large scales, 7.3-7.4. Research activities in Atmospheric and Oceanic Modelling, edited by H.Richie, WMO/TD - No. 987, Report No. **30**. 7.3-7.4

Boer, G. J., 1984: A Spectral Analysis of Predictability and Error in an Operational Forecast System. *Mon. Wea. Rev.*, **112**, 1183-1197.

Boer, G. J., 1993: Systematic and Random Error in an Extended-Range Forecasting Experiment. *Mon. Wea. Rev.*, **121**, 173-188.

Caya, D. and S. Biner, 2004: Internal Variability of RCM Simulations Over an Annual Cycle. *Clim. Dyn.*, **22**, 33-46.

Caya, D. and R. Laprise, 1999: A semi-implicit semi-Lagrangian regional climate model: the Canadian RCM. *Mon. Wea. Rev.*, **127**, 341-362.

Christensen, O. B., M. A. Gaertner, J. A. Prego and J. Polcher, 2001: Internal Variability of Regional Climate Models. *Clim. Dyn.*, **17**, 875-887.

Davies, H. C., 1976: Lateral Boundary Formulation for Multi-level Prediction Models. *Quart. J. R. Met. Soc.*, **102**, 405-418.

Davies, H. C. and R. E. Turner, 1977: Updating Prediction Models by Dynamical Relaxation: an Examination of the Technique, *Quart. J. R. Met. Soc.*, **103**, 225-245.

De Elía, R., R. Laprise and B. Denis, 2002: Forecasting Skill Limits of Nested, Limited-Area Models: A Perfect Model Approach. *Mon. Wea. Rev.*, **130**, 2006-2023.

De Elía, R., D. Caya, H. Côté, A. Frigon, S. Biner, M. Gigueère, D. Paquin, R. Harvey and D. Plummer, 2007: Evaluation of uUncertainties in the CRCM-Simulated North American Climate. *Clim. Dyn.*, DOI 10.1007/s00382-007-0288-z.

Denis, B., R. Laprise, D. Caya and J. Cote, 2002: Downscaling Ability of One-Way Nested Regional Climate Models: The Big-Brother Experiment. *Clim. Dyn.*, **18**, 627-646.

Denis B., J. Côté and R. Laprise, 2002: Spectral Decomposition of Two-Dimensional Atmospheric Fields on Limited-Area Domains Using the Discrete Cosine Transform (DCT). *Mon. Wea. Rev.*, **130**,1812-1829.

Gates, W. L., 1992: AMIP: The Atmospheric Model Intercomparison Project. *Bull. American Meteor. Soc.*, **73**, (12), 1962-1970.

Giorgi, F. and G. T. Bates, 1989: The Climatological Skill of a Regional Climate Model over Complex Terrain. *Mon. Wea. Rev.*, **117**, 2325-2347.

Giorgi, F. and X. Bi, 2000: A Study of Internal Variability of a Regional Climate Model, *J. Geophys. Res.*, **105**, D24, 29503-29521.

Giorgi, F. and L. O. Mearns, 1999: Introduction to Special Section: Regional Climate Modeling Revisited, *J. Geophys. Res.*, **104**, D6, 6335-6352.

Jones, R. G., J. M. Murphy, M. Noguer and M. Keen, 1997: Simulation of Climate Change over Europe Using a Nested Regional-Climate Model. II: Comparison of Driving and Regional Model Responses to a doubling of Carbon Dioxide. *Quart. J. R. Meteorol. Soc.*, **123**, 265-292.

Kain, J. S. and J. M. Fritsch, 1990: A one dimensional entraining/detraining plume model and its application in convective parameterizations. *J. Atmos. Sci.*, **47**, 2784-2802.

Kalnay, E., M. Kanamitsu, R. Kistler, W. Collins, D. Deaven, L. Gandin, M. Iredell, S. Saha, G. White, J. Woollen, Y. Zhu, A. Leetmaa, B. Reynolds, M. Chelliah, W. Ebisuzaki, W. Higgins, J. Janiwiak, K. C. Mo, C. Ropelewski, J. Wang, R. Jenne and D. Joseph, 1996: The NCEP/NCAR 40-Year Reanalysis Project, *Bull. American Meteor. Soc.*, **77**, (3), 437-471.

Laprise, R., D. Caya, D. Bergeron and M Giguère, 1997: The formulation of André Robert MC2 (Mesoscale Compressible Community) model. The André J. Robert Memorial Volume (C. Lin, R. Laprise, and H. Ritchie, Eds.), companion volume to *Atmos.-Ocean*, **35**, 195-220.

Laprise, R., M. R. Varma, B. Denis, D. Caya and I. Zawadzki, 2000: Predictability of a Nested Limited-Area Model, *Mon. Wea. Rev.*, **128**, 4149-4154.

Lorenz, E. N., 1969: The predictability of a flow which possesses many scales of motion. *Tellus*, **21**, 289-307.

Lorenz, E. N., 1982: Atmospheric predictability experiments with a large numerical model. *Telluss*, **34**, 505-513.

Miguez-Macho, G., G. L. Stenchikov and A. Robock, 2004: Spectral nudging to eliminate the effects of domain position and geometry in regional climate simulations. *J. Geophys. Res.*, **109** (D13), D13104, 10.1029/2003JD004495

Riette, S. and D. Caya, 2002: Sensitivity of short simulations to the various parameters in the new CRCM spectral nudging. Research activities in Atmospheric and Oceanic Modelling, edited by H. Ritchie, WMO/TD - No 1105, Report No. 32: 7.39-7.40.

Rinke, A., P. Marbaix, and K. Dethloff, 2004: Internal Variability in Arctic Regional Climate Simulations: Case Study for t he Sheba year. *Climate Res.*, **27**, 197-209.

Robert, A. and E. Yakimiw, 1986: Identification and elimination of an inflow boundary computational solution in limited area model integrations. *Atmos.-Ocean*, **24**, 369-385.

Schubert, D. and M. Suarez, 1989: Dynamical Predictability in a Simple General Circulation Model: Average Error Growth. *J. Atmos. Sci.*, **46**, 353-370.

Van Tuyl, A. H., and R. M. Errico, 1989: Scale Interaction and Predictability in Mesoscale Model. *Mon. Wea. Rev.*, **117**, 495-517.

Von Storch, H., H. Langenberg and F. Feser, 2000: A spectral nudging technique for dynamical downscaling purposes. *Mon. Wea. Rev.*, **128**, 3664-3673.

Vukicevic, T. and R. M. Errico, 1990: The Influence of Artificial and Physical Factors upon Predictability Estimates Using a Complex Limited-Area Model. *Mon. Wea. Rev.*, **118**, 1460-1482.

Vukicevic, T. and J. Paegle 1989: The Influences of One-Way Interacting Lateral Boundary Conditions upon Predictability of Flow in Bounded Numerical Models. *Mon. Wea. Rev.*, **117**, 340-350.

Weisse, R., H. Heyen and H. von Storch, 2000: Sensitivity of a Regional Atmospheric Model to a Sea State-Dependent Roughness and the Need for Ensemble Calculations. *Mon. Wea. Rev.*, **128**, 3631-3643.

Yakimiw, E. and A. Robert, 1990: Validation experiments for a nested grid-point regional forecast model. *Atmos.-Ocean*, **28**, 466-472.